A reassessment of outer-rise seismicity and its implications for the mechanics of oceanic lithosphere

Article *in* Geophysical Journal International · March 2014

DOI: 10.1093/gji/ggu013

CITATIONS
47

READS
803

3 authors, including:

Timothy Craig
University of Leeds
31 PUBLICATIONS **550** CITATIONS

SEE PROFILE

Jordan Jackson
George Mason University
41 PUBLICATIONS **766** CITATIONS

SEE PROFILE

Geophysical Journal International

Geophys. J. Int. (2014) doi: 10.1093/gji/ggu013

Geophysical Journal International Advance Access published February 14, 2014

A reassessment of outer-rise seismicity and its implications for the mechanics of oceanic lithosphere

T. J. Craig,[1,2] A. Copley[1] and J. Jackson[1]

[1]*COMET+, Bullard Laboratories, Department of Earth Sciences, University of Cambridge, Madingley Road, Cambridge, CB3 0EZ, UK.*
E-mail: craig@geologie.ens.fr
[2]*Laboratoire de Géologie, Ecole Normale Supérieure, 24 rue Lhomond, F-75231 Paris Cedex 05, France*

Accepted 2014 January 13. Received 2014 January 13; in original form 2013 October 7

SUMMARY

We use body-waveform modelling to constrain the source parameters of earthquakes occurring globally in oceanic lithosphere beneath the subduction zone outer rise and outer trench slope. These data are then used to map the stress state in the lithosphere of the downgoing plate as it bends into the subduction zone. Our results provide new constraints on the faulting of oceanic lithosphere at the outer rise, which is important for understanding the transmission of plate-driving forces through the subduction system. In all cases, shallow normal-faulting earthquakes are observed at the top of the plate, and are separated in depth from any deeper thrust-faulting earthquakes. No temporal variation associated with large thrust-faulting earthquakes on the subduction interface is seen in the depth extent of each type of faulting at the outer rise. The transition depth from trench-normal extension to compression is found to vary in agreement with models in which deformation is driven by the combination of in-plane stresses and bending stresses, resulting principally from slab pull. Combining the seismologically derived constraints on the thickness of the elastic core of the plate with estimates of the plate curvature, we place upper bounds on the strength of the lithosphere at the outer rise, which is required to be $\lesssim$300 MPa for a constant yield stress model, or governed by an effective coefficient of friction of $\lesssim$0.3.

Key words: Earthquake source observations; Rheology and friction of fault zones; Dynamics and mechanics of faulting; Lithospheric flexure; Rheology: crust and lithosphere.

1 INTRODUCTION

Beneath the outer rise and outer trench slope at subduction zones, the incoming plate bends down into the trench in response to compressive stresses transmitted across the subduction interface and to buoyancy-driven forces acting on the descending oceanic lithosphere. This bending results in varying degrees of shallow normal faulting and deeper thrust faulting within the plate (e.g. Stauder 1968a; Chapple & Forsyth 1979; Lay *et al.* 2009). Given the large seismogenic thickness of old oceanic lithosphere, earthquakes in such settings have the potential to be high magnitude ($M_W \geq 8$), and are occasionally tsunamigenic. This study investigates the seismicity beneath the outer rise and outer trench slope in the majority of regions around the world where significant outer-rise seismic activity has occurred within the instrumental period (Fig. 1), and examines what this seismcity can tell us about the deformation and strength of the plate.

Seismicity related to the bending of oceanic plates was first recognised by Stauder (1968a) along the Aleutian arc, and since then has been the subject of a number of global studies (e.g. Chapple & Forsyth 1979; Forsyth 1982; Christensen & Ruff 1988), along with specific studies of individual earthquake sequences for major outer-rise earthquakes (e.g. Kanamori 1971; Abe 1972; Lynnes & Lay 1988; Tichelaar *et al.* 1992; Ammon *et al.* 2008; Lay *et al.* 2010). Extensive studies have been conducted on many of the largest outer-rise earthquakes. However, although these events represent a significant proportion of the overall moment release, their relative scarcity results in limited spatial coverage. To attain the spatial coverage which is important when trying to assess global patterns in the outer-rise stress state, it is necessary to also consider smaller magnitude events.

The principal focus of this work is to present new observations for earthquake source mechanisms and depths constrained by waveform modelling within the oceanic plate seaward of subduction zones, with the intention of mapping out the stress state within the oceanic lithosphere in the near-trench environment. Substantial areas of the outer trench slope and outer rise of many subduction zones show little or no major seismicity (e.g. west of Peru and in the Caribbean). Fig. 1 outlines the regions covered in this study, where significant outer-rise seismicity has been observed during the instrumental period. In regions with sufficient seismicity, it is possible to estimate the transition depth from extension to compression within the plate.

It has been suggested that temporal variations in the stress transmitted across the adjacent subduction interface over the seismic

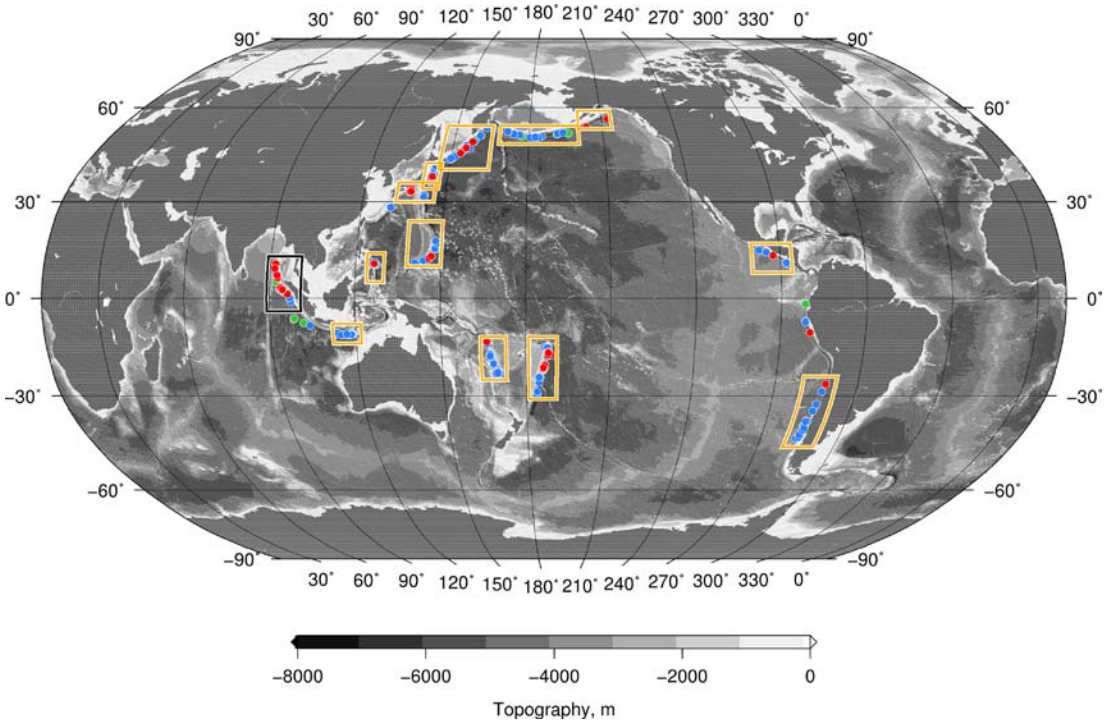

Figure 1. Global outer-rise seismicity. Bathymetric map, showing the regions of focus in this study. Outer-rise earthquakes with accurately constrained source parameters are given by the coloured circles. Earthquakes are coloured by mechanism: thrust faulting—red; normal faulting—blue; strike-slip faulting—green. Boxes outline the regions covered in this work (orange), and by a companion study (black; Craig & Copley, in preparation).

cycle modulates the near-trench seismicity in the downgoing plate (Christensen & Ruff 1983, 1988; Lay *et al.* 2009). In this conceptual model, normal-faulting earthquakes in the downgoing plate become progressively inhibited as stress builds up on the subduction interface, and are enhanced following its release, with the converse being applied to compressional earthquakes. However, the recent occurrence of a major outer-rise extensional earthquake just prior to a megathrust event in Tonga (Lay *et al.* 2010), and of large magnitude compressional aftershocks beneath the outer rise following megathrust events in the Kurils and Japan (Lay *et al.* 2009, this study), calls into question the degree to which this effect influences seismicity within the downgoing oceanic plate. We will examine the temporal evolution of outer-rise seismicity as part of this study.

A further aim of this work is to use our earthquake data set to investigate the material properties of the faults within oceanic lithosphere at the outer rise of subduction zones. The factors controlling the distribution and style of faulting in the downgoing plate at the outer rise, and how these are reflected in the observed seismicity, are also discussed.

This study first presents new observations of earthquake source mechanisms and depths within the oceanic plate seaward of subduction zones. Each subduction zone in which significant seismic activity in the outer rise has been observed is considered in terms of the spatial and temporal distribution of seismicity. The relationship between seismicity in the downgoing plate and seismic activity on the main subduction interface is then assessed, and the implications of these intraplate earthquake observations for our understanding of the rheology of oceanic lithosphere, the influence of plate driving forces on intraplate deformation, and the relationship between bending-related seismicity and the thermal structure of oceanic lithosphere, are discussed. The rheological properties of the plate are then studied by considering the accumulation and accommodation of strain within the bending plate.

This study presents a total of 147 new earthquake source models across 12 regions, which are combined with further earthquakes with well-determined source parameters compiled from the literature. Full solutions for all new events are given in Table S1. Recent studies have focused on the characteristics of individual earthquake sequences, typically dominated by a major earthquake (e.g. Lay *et al.* 2009, 2010). Instead of focusing on a single region, this study instead takes a more global perspective, seeking to understand the differences and similarities in outer-rise seismicity between regions.

2 MECHANICAL MODELS OF THE OUTER RISE

Bending-related seismicity is often referred to as ‘outer-rise’ seismicity, but earthquakes in fact rarely occur beneath the outer rise. Instead most are confined to the outer trench slope with the majority of earthquake activity within ∼75 km of the trench axis (coincident with the region of highest plate curvature, and the resultant concentration of strain; see Section 10, and Fig. S1). This distribution is predicted by models of plastic failure of the plate close to the trench, when the bending stresses become sufficient to permanently deform the oceanic lithosphere (Chapple & Forsyth 1979; Forsyth 1980). The proximity of the seismicity to the trench, indicative of the majority of strain being focused within a relatively short horizontal extent, can be most easily explained using a rheological model with an elastic core bracketed by regions undergoing plastic failure, if this plastic failure can be taken as a long-term approximation to elastic strain build-up and release on faults (Forsyth 1980).

The stress-state of a given point within the incoming oceanic lithosphere is expected to vary with both distance from the trench and depth within the lithosphere, due to the changing pattern of bending stresses as the incoming plate approaches the trench. The

stress state within the lithosphere in this relatively simple deformation setting can be inferred from the style of faulting seen in the earthquake focal mechanisms at a given point (i.e. thrust or normal faulting). However, accurate depth determination for earthquakes beneath the outer trench slope is difficult. The resolution of routine methods, whether based on traveltimes, surface waves or very long period body-waves, is insufficient to constrain the depth of earthquakes with the accuracy required to distinguish confidently between compressional and extensional regions distributed over the thickness of the seismogenic part of the plate ($\leq$60 km). Only by the careful analysis of body-waveform data can accurate measurements of earthquake depths within the plate be made (e.g. Forsyth 1982). We therefore use the modelling of body-waves in this study to determine focal mechanisms and depths for earthquakes at the outer rise, and map out the stress state in downgoing lithosphere close to the subduction trench.

In an elastic-plastic model, as has been previously used to explain outer-rise bathymetry and seismicity (e.g. M^{c}Adoo *et al.* 1978; Chapple & Forsyth 1979; Forsyth 1980), plastic deformation occurs when the stress within the lithosphere exceeds a pre-defined yield stress. The stress limit which marks the onset of plastic deformation as a function of depth defines a yield stress envelope. The depth integration of this yield stress envelope, and any deeper ductile support of stresses, determines the total strength of the plate. Where the stress does not exceed that supportable on faults, the plate behaves elastically; when it does, it will behave plastically. In an elastic-plastic layer, when subjected to bending stresses, the top will experience extension, and the base compression. The greatest stresses, and hence the initial points of plastic failure, will occur at the top and bottom of the elastic-plastic layer, separated by a region which will continue to behave elastically (referred to hereafter as the elastic core). It is the thickness of, and stress gradient within, this elastic core which governs the flexure of the plate (Caldwell *et al.* 1976; Chapple & Forsyth 1979), both of which are dependent on the yield stress envelope of the plate, and the amount of bending.

The presence of any in-plane stresses, in addition to the bending stress, will move the position of the elastic core up (if the in-plane stress is horizontally compressive) or down (if the in-plane stress is horizontally extensional). Hence, this position of the transition from horizontal extension to horizontal compression potentially contains information about both the rheological structure of the plate, and the applied in-plane stresses. By combining seismological constrains on the depth of the elastic core with observations of the plate deflection, we can place bounds on the rheological structure of the lithosphere. Previous studies have attempted to use the combination of seismological and deflection data to constrain the applied stresses by assuming a rheological profile for the plate (e.g. Liu & M^{c}Nally 1993). However, given continuing uncertainty about the way in which the lithosphere supports stresses, we take the approach of simply trying to constrain the strength of the lithosphere, without determining the magnitudes of the various far-field stresses acting on the system.

3 SEISMICITY OF THE OUTER TRENCH SLOPE AND OUTER RISE

3.1 Earthquake source modelling

Distinguishing earthquakes within the oceanic plate beneath the outer rise and trench slope from those on the subduction interface is relatively simple, based on the seismologically determined location relative to the bathymetric trench. In this study, we use the locations of Engdahl *et al.* (1998) if available, or the NEIC if not. Once the depth of an earthquake is accurately determined, this further distinguishes events within the plate from interplate events along the interface between the converging plates.

The accurate determination of earthquake source parameters for moderate sized earthquakes in oceanic settings, and particularly near subduction zones, requires careful waveform modelling. The presence of high-impedance-contrast layering relating to near-source sediments and the overlying water layer, and the multiples that result from both, make interpretation of the observed phases for body-wave data, particularly *P*-wave data, complex, as the correct identification of phases is often difficult (e.g. Forsyth 1982). In addition, the lack of information about the relative impedances of the various layers below the seabed makes the determination of relative amplitudes for reflected phases uncertain. When handling data from a range of azimuths from a single earthquake, source modelling is further complicated by azimuthal variations in the source-side velocity structure, principally in water depth, making the relative time delay between various phases azimuth dependent. The simple Greens functions calculated from a 1-D velocity model used in our modelling approach do not take the 3-D structure of the source-side velocity structure and its associated interfaces into account, and as such the effects of this on the delay times and relative amplitudes of the depth phases are not taken into account in our solutions. However, this effect is relatively minor when compared to other sources of uncertainty (such as the overall velocity model), and where good azimuthal data coverage exists, it can often be manually compensated for to a certain degree.

To minimize these difficulties, particularly those relating to the velocity structure, the assessment of earthquake source parameters in this study is restricted to those earthquakes large enough to generate sufficient energy to allow analysis at periods $\gtrsim$1 s. This limitation on the frequencies used helps to remove the effects of short-wavelength variations in the velocity structure, relating to shallow sediment layers. Additionally, the use of shear-wave data—which do not pass through the water layer, and hence are not complicated by water multiples—in source determination becomes critical for correctly differentiating between the seabed reflection and water multiples in *P*-wave data.

The modelling strategy used is similar to that employed extensively in the literature (e.g. Taymaz *et al.* 1991; Tilmann *et al.* 2010), using the algorithm of Zwick *et al.* (1994) to invert *P*- and *SH*-wave data at teleseismic distances, approximating the earthquake source as a point source with a finite-duration source-time function. A simple velocity structure is used, consisting of a crustal layer 7 km thick ($V_p = 6.5$ m s^{-1}, $V_s = 3.8$ m s^{-1}, $\rho = 2800$ kg m^{-3}) overlying a mantle halfspace ($V_p = 8.1$ m s^{-1}, $V_s = 4.6$ m s^{-1}, $\rho = 3300$ kg m^{-3}). Given that the sediment thickness and velocity structure are poorly constrained for the majority of subduction regions around the world, rather than trying to incorporate a separate sediment layer, this is approximated by having a slightly slower crustal velocity structure than is typical for oceanic lithosphere. As the majority of events we study are deeper than the interface at the base of the crustal layer, and the thickness of the sediment layer is small compared to the wavelength of the body-waves used, this approximation will not have a significant effect on our results. For each earthquake, the velocity model is overlain by a water layer with the depth in the source region being initially based on the SRTM30PLUS bathymetric model (filtered to remove wavelengths $<$10 km), and adjusted as required to best fit any observed water multiples. The onset of the direct phase—the start of the inversion window used—is in each

case picked from the broadband seismogram where possible. Discarding the absolute traveltimes, and only considering the relative delay between direct and depth phases, removes any dependence of our results on the receiver-side velocity structure.

Typical errors in source parameters using this method are $\sim\pm10^\circ$ for strike and rake, and $\sim\pm5^\circ$ for dip (e.g. Taymaz *et al.* 1991; Tilmann *et al.* 2010). Of particular relevance to this study are uncertainties in depth which are typically ±3–4 km for earthquakes with $M_W \leq 5.5$. In the case of the outer rise, it is often necessary to model larger magnitude events ($M_W \geq 7$) for which depth estimates trade-off significantly with the duration and shape of the source-time function. In cases where the magnitude exceeds M_W 7, the uncertainties in centroid depth can be up to $\pm\sim$10 km.

For a small number of lower magnitude ($M_W \leq 5.5$) earthquakes, the signal-to-noise ratio at a small number of stations was sufficient to allow the identification of multiple depth phases, but the earthquake either failed to generate sufficient energy at long periods, or the number of stations with clear signals above the level of the background noise was too small, to allow a full inversion as described above. In those cases, a depth estimate was then calculated by iterative forward-modelling of the principal depth phases using the WKBJ algorithm (Chapman *et al.* 1988). These events are labelled in Table S1, and the mechanism is taken from the gCMT catalogue.

3.2 Earthquake catalogues

For the most complete picture of outer rise and outer-trench-slope seismicity, it is necessary to consult a range of earthquake catalogues, in addition to our own source modelling.

In considering the temporal activity in the outer rise, the results of the gCMT catalogue (www.globalcmt.org) are included for events which are too small or too noisy to be modelled using the techniques employed here, covering a period from 1967 March 27 to 2013 July 31, although the catalogue completeness changes over that time period. While the depth resolution in this catalogue is insufficient for the purposes of accurately constraining the boundary between normal- and thrust-faulting earthquakes in depth, the epicentral locations and mechanisms are sufficient for use in analysing the temporal relationship between activity on the interface and within the adjacent downgoing plate. For instrumentally recorded events for which locations and focal mechanism, or at least mechanism type, are known, but which are not included in the gCMT catalogue (typically those prior to 1975), the compilation of Christensen & Ruff (1983) is used.

The along-strike extent of major ($M_W > 7.5$) interface events during the instrumental period is based on published studies from the literature, or estimated based on the area encompassed by aftershocks occurring within a 1 month period after the main shock, and recorded in the NEIC catalogue. For older events, where rupture lengths have been estimated from historical, geological or palaeoseismological sources, or based on specific studies of sparse early seismic records, rupture lengths are taken from the individual published studies, and from the compilations of Rhea *et al.* (2010).

A number of recent major earthquakes have been modelled using finite-fault inversion algorithms to estimate the slip distribution on the fault plane (e.g. Ammon *et al.* 2008; Lay *et al.* 2010). Where appropriate, these are incorporated into the database compiled here.

In a number of places, most notably offshore central America and east of Honshu, accurate micro-earthquake studies utilizing ocean-bottom seismometers have been conducted (Lefeldt *et al.* 2009; Hino *et al.* 2009; Obana *et al.* 2012), and the results of these are again incorporated into our study.

4 REGIONAL SEISMICITY

Sections 4.1 to 4.10 present the seismicity of each region where significant outer-rise seismicity has been observed. Earthquakes with well-determined source parameters are presented as focal mechanisms, along with the best-fit depth below the seafloor. Major ($M_W \geq 7.0$) interface events are also shown, taken from the gCMT catalogue. Where large outer-rise earthquakes have occurred, the best available solution is shown—finite-fault if possible (taken from other studies), or point-source (in this study or others as given in the figure caption and text) if not. In cases where major ($M_W \geq 7.0$) outer-rise events have occurred, but accurate source parameters are hard to determine (either due to source complexity or due to data availability) the gCMT mechanism is shown, along with the NEIC centroid depth (which is likely to be a more reliable estimation of the earthquake depth than that from the gCMT, due to the inclusion of higher frequencies). Small triangles are plotted for all earthquakes in the gCMT catalogue occurring within 150 km seaward of the bathymetric trench line (shown in white on all figures). The local convergence vector across the interface, from the MORVEL plate model (DeMets *et al.* 2010), is also plotted for the downgoing plate relative to the overriding plate. For most regions the distribution of outer-rise and major interface seismicity is also shown as function of latitude or longitude, from 1960 to present. Major interface seismicity prior to 1960, if known, is also indicated along the side of the plot, although for many island arcs, knowledge of the interface seismicity prior to the 1960s is limited.

After discussing the seismicity of each region in turn, we will then interpret the seismicity in the context of the plate rheology and driving forces.

4.1 The Aleutian arc

Outer-rise seismicity along the Aleutian arc was first noted by Stauder (1968a,b) who identified a number of normal-faulting earthquakes occurring seawards of the trench. As Fig. 2 shows, the vast majority of seismicity within the oceanic plate seawards of the Aleutians is extensional—the principal exception being two compressional earthquakes at the eastern end of the arc (Fig. 2b). The majority of normal faulting earthquakes show a good correspondence between the orientation of the focal mechanism and the local strike of the trench. In contrast, the two thrust-faulting earthquakes both occur at an oblique angle to the strike of the trench, and are both significantly further seawards than the observed extensional activity further west. Hence, the identification of these thrust earthquakes as 'outer rise' remains open to question.

The main subduction interface has been seismically quiescent in terms of major earthquakes since the end of a sequence rupturing much of the length of the arc from 1938 to 1965. As the record of outer-rise seismicity only covers the period after this sequence, making any statements about the time-dependence of seismicity along the Aleutian outer rise is difficult. However, the largest outer-rise normal-faulting earthquake, a M_W 7.2 event in 1965 (Abe 1972, light blue mechanism, Fig. 2), occurred directly seawards of the interface rupture occurring in the 1965 M_W 8.7 Rat Islands Mainshock, and only 54 days after the interface main shock. Abe (1972) conducted detailed surface-wave studies of this earthquake to determine the mechanism, and, based on its aftershock distribution, concluded

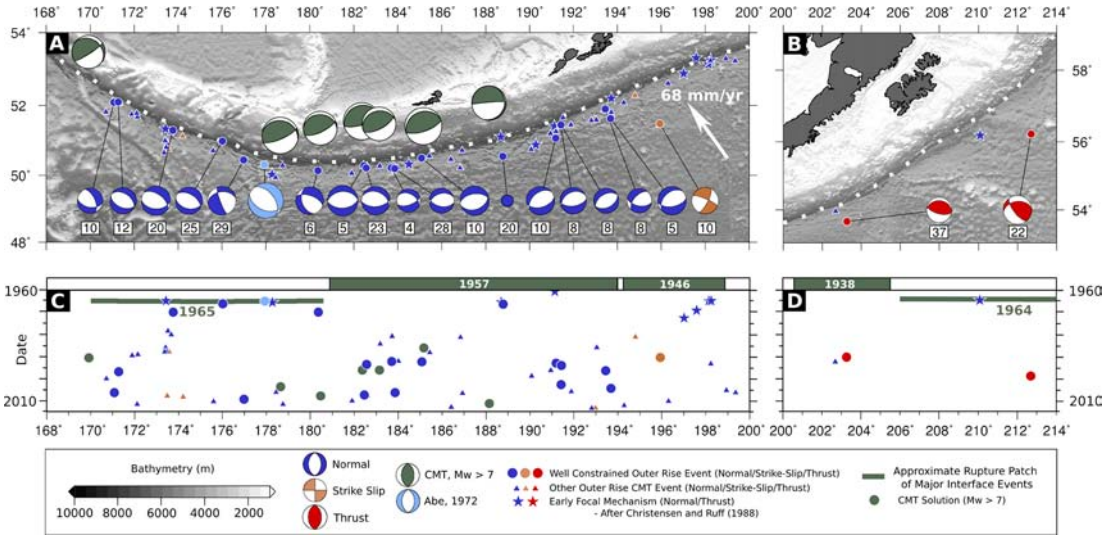

Figure 2. Outer-rise seismicity along the Aleutian arc. (a) Seismicity along the western/central Aleutians. Focal mechanisms in this and subsequent figures are coloured by the style of deformation—blue, normal-faulting earthquakes; red, thrust-faulting earthquakes; and brown, strike-slip-faulting earthquakes. Green events indicate $M_W > 7.0$ events occurring landward of the trench—typically interplate thrust events. In cases where no mechanism is shown, this is due to the relevant study only determining earthquake depth through depth-phase analysis, and not independently determining a source mechanism. The centroid depth relative to the seafloor is given in the box beside each earthquake. The light blue focal mechanism is that of Abe (1972) for the M_W 7.2 1965 Rat Islands earthquake. The depth of this earthquake is uncertain, and hence not shown. Earthquakes are included from Herrmann (1976); Chapple & Forsyth (1979); Forsyth (1982); Jaumé & Estabrook (1992). (b) Limited seismicity along the eastern Aleutians, offshore Alaska. (c) Time versus longitude plot for the western/central Aleutians. (d) Time versus longitude plot for the eastern Aleutians. Bars along the top of (c) and (d) indicate pre-1960 interface seismicity.

that the earthquake ruptured through the entire lithosphere, down to an estimated ∼70-km depth. However, it is notable that no other extensional earthquake along the arc for which a well determined depth is known is deeper than 30 km. Given that the conclusion of Abe (1972) was based on routine ISC earthquake depths for low-magnitude aftershocks, which often have large uncertainties, and the lack of any other supporting evidence, we conclude that while the lithosphere at the western end of the arc appears to be entirely in extension over the depth range undergoing brittle failure, the presence of seismicity down to the great depths inferred by Abe (1972) remains uncertain.

4.2 The Kurils-Kamchatka trench

Outer-rise seismicity along the Kurils (Fig. 3) is dominated by a sequence following a M_W 8.3 interplate event on 2006 November 15. This was followed by an aftershock sequence in the adjacent outer rise and trench slope region, peaking in a M_W 8.1 normal-faulting earthquake on 2007 January 13, and a M_W 7.4 deep thrust event on 2009 January 15 (Ammon *et al.* 2008; Lay *et al.* 2009). The main extensional event had slip concentrated in the top 22–29 km of the oceanic plate (Lay *et al.* 2009), with a sharp gradient of decreasing slip with depth. The subsequent compressional event has a poorly constrained depth, principally due to its large magnitude and the associated trade-offs between depth and source duration. Lay *et al.* (2009) determined rupture occurring within the depth range from 35 to 55 km. Point-source centroid modelling using the techniques employed here agrees with this estimate, with a minimum misfit centroid depth of 42 ± 8 km below the sea surface.

The 2006 interface event was preceded by a compressional event in the outer rise in 1963 (red star at 46.8°N, 154.8°E, Fig. 3). Analysis of sparse long-period waveform data by Raeesi & Atakan (2009) indicates a depth of ∼35 km for the 1963 compressional outer-rise earthquake, although, given the magnitude, this is subject to significant trade-off against the source duration, and the precise depth is not well defined. While the actual depths are relatively poorly constrained for these deeper compressional events, they do illustrate two important concepts. First, following the major interface event, the outer rise remains capable of compressional failure at depth. Secondly, the depth extent over which compressional failure occurs may not have changed significantly from before to after the interface event, although without the observation of further earthquakes, this is difficult to confirm.

Prior to the sequence from 2006 onwards, the majority of outer-rise activity along the Kurils-Kamchatka trench was a group of tensional earthquakes seaward of the rupture patch of the 1963 M_W 8.5 Kuril interface event. This 1963 earthquake was followed by continuing activity both on the interface and within the adjacent oceanic plate. The junction between the 1963 interface rupture patch, and the area that ruptured in the 2006 interface event, is marked by the presence of two compressional, and relatively deep, outer-rise events occurring in the period between earthquakes.

The northern end of the trench, seaward of the 1952 M_W 9.0 Kamchatka interface event is marked by very little outer-rise activity. There are a small number of extensional earthquakes, and a single relatively shallow thrust earthquake at the southern end of the 1952 rupture patch.

4.3 Japan

The Japan trench, east of Honshu, is one of the most seismically active outer-rise and outer-trench-slope regions (Fig. 4). The recorded history of instrumental seismicity along this stretch of oceanic lithosphere extends back to the M_W 8.6 Sanriku earthquake of 1933 (Kanamori 1971). This major outer-rise extensional event ruptured the oceanic lithosphere seawards of the approximate location of a large subduction earthquake (the 1896 M_W 8.5 Meiji-Sanriku earthquake; Kanamori 1972). The depth extent of the 1933

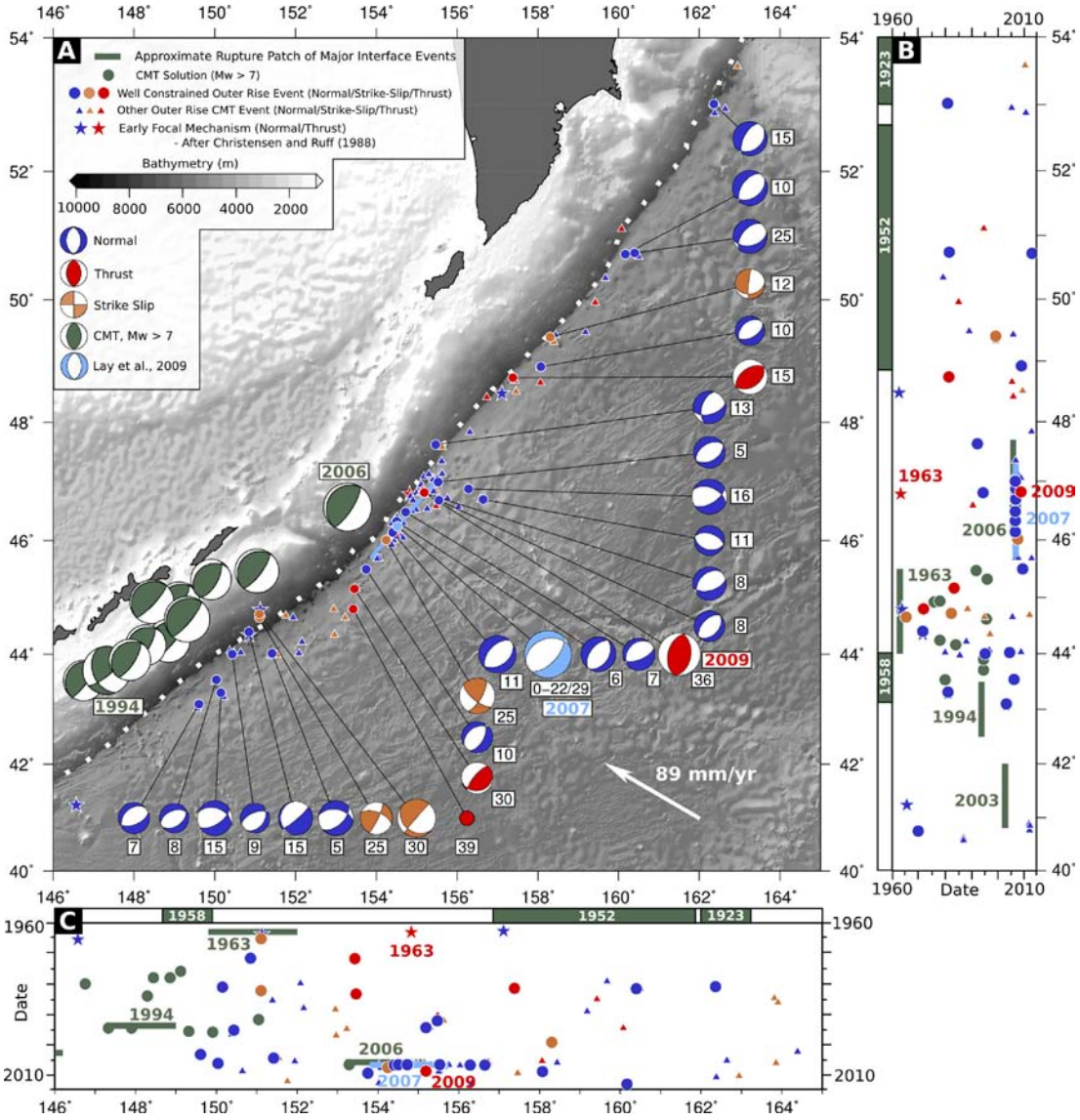

Figure 3. Outer-rise seismicity along the Kurils-Kamchatka trench. (a) Seismicity and earthquake focal mechanisms. The light blue focal mechanism is that of Lay *et al.* (2009) for the 2007 M_W 8.1 Kuril Islands earthquake, with the light blue bar denoting the along-strike extent of their preferred finite-fault model. Earthquakes are included from Fitch *et al.* (1981); Forsyth (1982); Liu & M^{c}Nally (1993); Seno & Yamanaka (1996); Raeesi & Atakan (2009). (b) Time versus latitude plot. (c) Time versus longitude plot.

rupture is not well constrained. Kanamori (1971) suggests, on the basis of standard scaling relationships, that the 1933 earthquake ruptured the entire thickness of the lithosphere. However, such relationships assume knowing the stress drop and length of the rupture, both of which are hard to estimate. Subsequent (and continuing) aftershocks in the source region only reach to depths of ∼25 km (Hino *et al.* 2009; Gamage *et al.* 2009), indicating that rupture was perhaps confined to the upper lithosphere only.

In the late 20th century, outer-rise seismicity was more sparse along this margin, with a number of small normal-faulting earthquakes down to depths of 20 km, and a single well-determined thrust-faulting earthquake at 41 km (Seno & Gonzalez 1987). Seno & Gonzalez (1987) also report an earthquake at 31 km, which they interpret as extensional. However, their mechanism, constrained only by first-motion polarities from limited data, can also be compatible with a strike-slip source, and so is excluded from the compilation presented here. On the 2011 March 11, the M_W 9.0 Tohoku-Oki earthquake ruptured ∼500 km of the subduction interface along the Japan trench. The second largest aftershock in the immediate post-earthquake period, occurring ∼ 40 min after the main shock, was a M_W 7.7 outer-rise normal fault (purple mechanism, Fig. 4). The signal from this earthquake is obscured by the continuing coda of the main shock, and this prevents an accurate determination of the depth (depth on Fig. 4 is taken from the NEIC catalogue). As Fig. 4(b) shows, the area adjacent to the slip patch of the Tohoku-Oki earthquake has since experienced numerous outer-rise aftershocks, dominantly extensional. It is notable that the highest concentration of activity is directly seawards of the highest patches of slip in the main shock, and hence in the region in which the largest change in stress state is expected from before to after the main shock.

While the majority of seismic activity is extensional, one particular event has a complex mechanism, incorporating a thrust-faulting component. On 2012 December 7, a M_W 7.2 earthquake occurred beneath the outer-trench-slope seawards of the high-slip

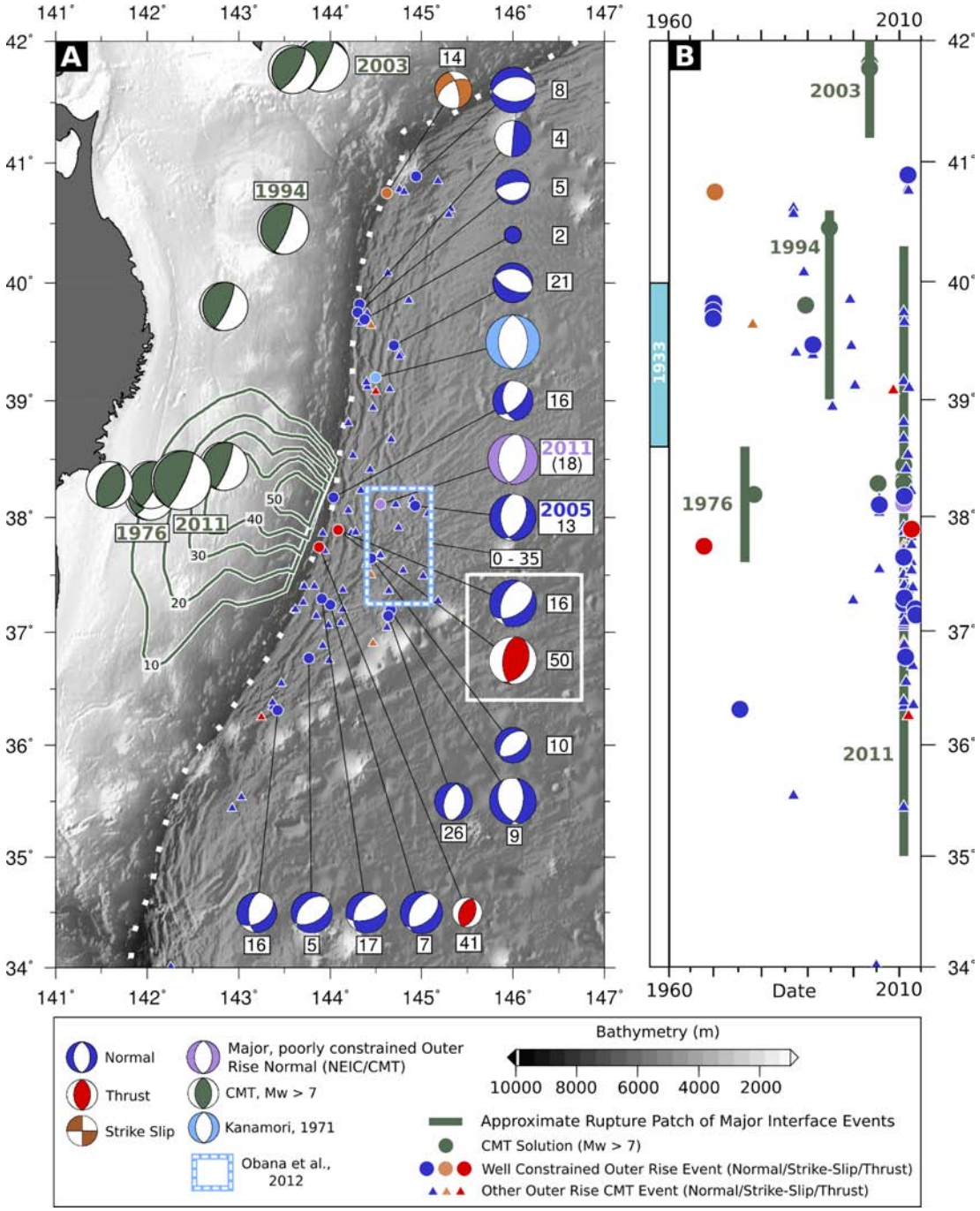

Figure 4. Outer-rise seismicity east of Honshu. (a) Seismicity and focal mechanisms. The region outline by the dashed box is that of the local OBS survey of Obana *et al.* (2012). The light blue mechanism is that of Kanamori (1971) for the 1933 Sanriku earthquake. The two mechanisms in the white box are the composite focal mechanisms of 2012 December 07 doublet. Green contours are slip contours for 2011 March 11 M_W 9.0 Tohoku-Oki earthquake at 10 m increments (Yue & Lay 2011). Earthquakes are included from Chapple & Forsyth (1979); Forsyth (1982); Seno & Gonzalez (1987); Seno & Yamanaka (1996). (b) Time versus latitude plot. The blue bar represents the approximate along-strike extent of the 1933 Sanriku event (Rhea *et al.* 2010).

patch in the main shock. To explain the observed waveforms from this earthquake, a composite mechanism, combining an initial deep (50 ± 4 km) thrust fault with a subsequent shallower (∼16 km) normal fault is required (mechanisms in white box, Figs 4 and 5; also Harada *et al.* 2013; Lay *et al.* 2013). The depth of the subsequent extensional rupture is not well constrained, and trades-off significantly against the onset time relative to the initial rupture in the compressional event. However, the extensional event is constrained to be shallower than the initial compressional event, with the minimum of the broad misfit function in depth lying at 16 km beneath the seafloor. Fig. 5(a) shows waveform modelling results for this event, modelling the source as a pair of point-source centroids. Fig. 5(b) shows a selection of waveforms for the individual thrust- and normal-faulting components of the best-fit solution, the composite solution, an inversion for a double-source thrust event, and an inversion for a single source thrust-faulting event with a long-duration source time function, to demonstrate the necessity of the subsequent normal-faulting event to fit the observed waveforms.

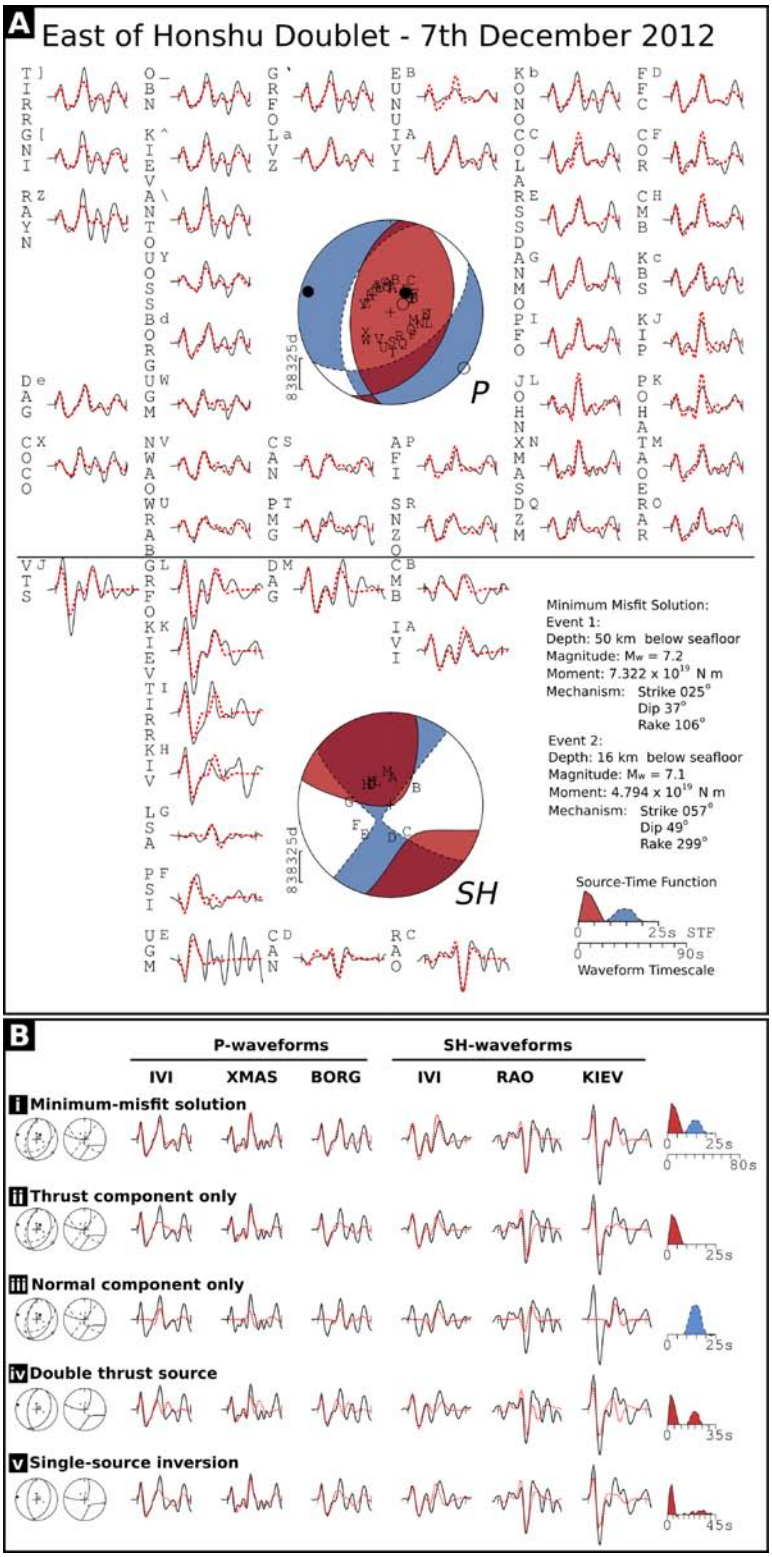

Figure 5. Waveform modelling solution for 2012 December 7 East of Honshu Doublet. Figure on previous page. (a) Minimum misfit solution for a two point source solution, located at 37.9°N, 144.1°E. The depth of the first (thrust) event is well constrained (red mechanism), the depth of the subsequent normal-faulting event (blue mechanism) trades-off against the time-delay between ruptures, but is shallower than the initial thrust. All parameters in the minimum misfit solution shown are left free to vary. On a number of the *SH* waveforms, the time window over which data are inverted for the earthquake source parameters (shown by the tick marks) is truncated to exclude the effect of core phase arrivals (e.g. KIV, UGM). (b) Sensitivity tests for the east of Honshu Doublet. In each case, three *P* and three *SH* waveforms are shown. (i) the minimum misfit solution shown in (a), (ii) The thrust-faulting part of the mechanism only, (iii) the normal-faulting part of the mechanism only, (iv) an inversion for a second thrust-fault source, with fixed mechanism and moment, but variable time-offset, and (v) a full inversion for a single-source solution, with all parameters free and the number of available source-time function elements in the inversion scheme for the event is increased allow the source-time function to encompass the duration of both episodes of moment release.

The results from our analysis match with those of other recent studies of the same earthquake sequence (Harada *et al.* 2013; Lay *et al.* 2013). This pair of earthquakes serve to highlight again that the outer rise can, in certain circumstances, remain in trench-normal compression at depth and capable of failure in thrust-faulting earthquakes following a major interface event, as also seen in the Kurils (see Section 4.2).

Along the Japan trench, a number of ocean-bottom seismometer surveys have been deployed to detect low-magnitude seismicity in the incoming Pacific plate (Hino *et al.* 2009; Obana *et al.* 2012). These studies have been focused on the expected aftershock areas of major outer-rise normal-faulting earthquakes. Aftershocks of the 2005 M_W 7.0 Sanriku earthquake (38.1°N, 144.9°E; Fig. 4), recorded in 2007, extend down to 20-km depth within the plate, with mechanisms consistent with the normal-faulting main shock (Hino *et al.* 2009). A small number of events in this region, at depths of ∼40 km have first-motion polarities consistent with compressional faulting, but the mechanisms are not well constrained. Seawards of the Tohoku-Oki slip patch, in the region of the 2011 M_W 7.6 outer-rise aftershock, the survey of Obana *et al.* (2012), conducted 1 month after the Tohoku-Oki earthquake and its M_W 7.6 normal-faulting aftershock, found normal-faulting micro-earthquakes extending to ∼30 km below the seafloor, along an alignment interpreted as the fault plane of the M_W 7.6 aftershock. No evidence of thrust-faulting earthquake activity was found in their local survey. It should be noted that the region encompassed by this survey is directly seaward of the 2012 doublet, which included compressional failure at depths of ∼50 km. A regional study, determining earthquake depths along the entire arc using *sP* delay times, found shallow extension down to 20 km, and compression between 32 and 43 km (Gamage *et al.* 2009).

The southern side of Honshu, along the Nankai trough (Fig. 6), is an area of complex seismicity in the downgoing plate. The outer trench slope shows very little seismic activity, with the gCMT catalogue reporting only a small number of relatively low magnitude ($M_W < 5.5$) normal and strike-slip faulting earthquakes. Beneath the trench itself, however, there is a cluster of high-angle thrust faulting earthquakes, offshore of the Kii Peninsula with depths ranging from 6 to 18 km within the young downgoing seafloor (Bai *et al.* 2007, this study, Fig. 6). This distribution of events is in agreement with the results of local OBS studies, which find microearthquakes extending from 5 to 26 km (Sakai *et al.* 2005; Bai *et al.* 2007). This group of high-angle thrusts in the oceanic plate occurs landwards of the Zenisu ridge, a bathymetric high running subparallel to the local trench, potentially formed as a result of intraplate thrusting (Lallemant *et al.* 1989) which, based on microseismic activity, is still active. Both shallow intraplate thrusting beneath the trench and active compressional faulting in the oceanic plate seaward of the trench may result from enhanced compressive stresses transmitted across the subduction interface by the collision of the thick crust of Izu Peninsula with southern Honshu to the northwest (Chamot-Rooke & Le Pichon 1989).

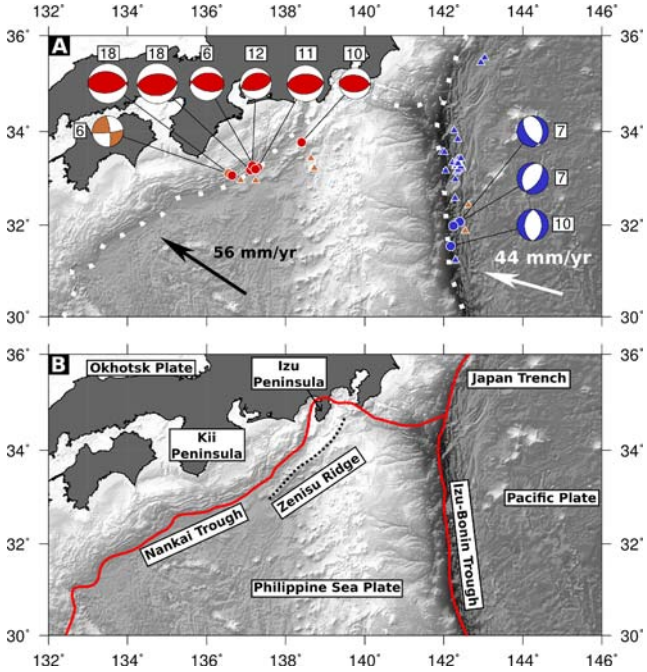

Figure 6. Near-trench seismicity along the northern Ryukyu and Izu-Bonin arcs. (a) Near-trench seismicity. White arrow is the velocity of the Pacific plate relative to the Philippine Sea Plate. Black arrow is the velocity of the Philippine Sea Plate relative to the Okhotsk plate. Catalogue seismicity seawards of the Nankai trench, but within ∼200 km of the Izu-Bonin and Japan trenches is excluded from the plot, due to complications in the tectonic environment in close proximity to the triple junction. Earthquakes are included from Bai *et al.* (2007). (b) Regional tectonics. Red lines indicate the subduction zones. Dotted black line indicates the basement high of the Zenisu ridge.

4.4 The Marianas arc

The Marianas arc (Fig. 7) represents an extreme case for outer-rise seismicity on several levels. First, the subduction interface itself has experienced far less moment release in major earthquakes than would be expected from the rate of convergence, with only a single $M_W \geq 7.0$ earthquake since 1975, suggesting that the interface is relatively uncoupled (e.g. Ruff & Kanamori 1980). Secondly, the slab dips into the mantle at a very high angle, approaching vertical within a short distance from the trench. The majority of the convergence at the subduction interface results from back-arc extension, perhaps associated with slab roll-back. Hence, bending strain along the direction of dip is expected to be high in order to achieve the steep dip angle of the slab and its relatively short radius of curvature. The kinematic picture in this region is further complicated by the 3-D nature of slab curvature in a subduction zone where the strike of the trench changes greatly along the length of the arc.

Seismicity in the downgoing plate along the length of the Marianas arc is dominated by shallow tensional earthquakes, with a general strike similar to the local orientation of the trench. Two deeper thrust-faulting earthquakes (at 40 and 42 km beneath the seafloor; Fig. 7) have been observed in the downgoing plate, both with orientations highly oblique to the orientation of the trench. The interplay of the different components of the 3-D stress field is hard to assess. However, a similar orientation of thrust earthquakes within the downgoing oceanic lithosphere with strikes oblique to a highly curved trench have been observed around the Hellenic arc and near Ryukyu, interpreted as along-strike shortening within the downgoing plate resulting from the increasing curvature of the downgoing plate with depth (Kao & Chen 1991; Shaw & Jackson 2010).

The largest recorded extensional event along the Marianas, a M_W 7.5 earthquake on 1990 April 5 at 15.1°N, 147.6°E, has been suggested by Zhang & Lay (1992) to represent the extensional failure of the entire vertical extent of the lithosphere. These authors

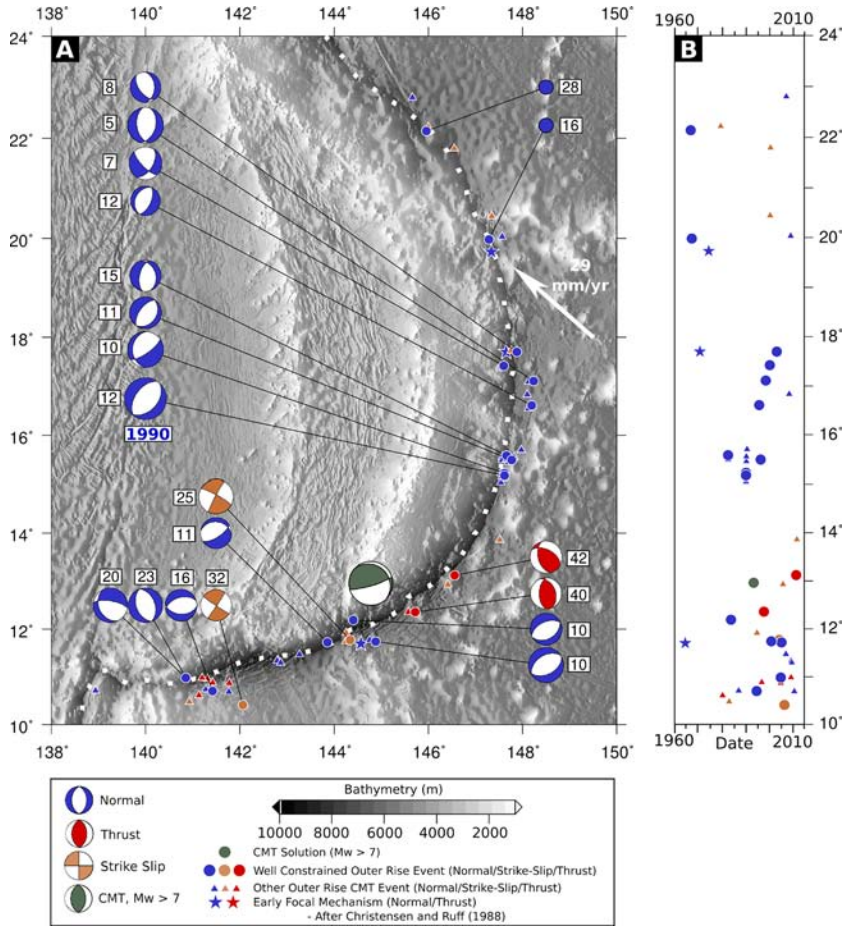

Figure 7. Outer-rise seismicity along the Marianas subduction zone. (a) Seismicity and focal mechanisms. Earthquakes are included from Zhang & Lay (1992); Seno & Yamanaka (1996). (b) Time versus latitude plot.

suggest that the location of this earthquake is at the junction between distinct segments of the subduction zone, and occurred as a result of high intraslab stresses induced by lateral distortions in the slab. While this earthquake and its aftershocks represent a significant majority of the seismic moment release observed in the outer rise of the Marianas, this may be the result of the short observation period ($\lesssim$100 yr).

A number of small (M_W < 5.5) compressional outer-rise earthquakes are present in the gCMT catalogue ($\sim$ 12.75°N 141.5°E), all with reported depths of 33–55 km. The strikes of the nodal planes of these earthquakes (not shown on Fig. 7), are $\sim$30° oblique to the strike of the trench, indicating that they are more compatible with compression aligned in an arc-perpendicular direction at depth within the plate than with trench-normal compression. Although accurate depth determination for such small earthquakes is problematic, and so the depths remain uncertain, the reported depths would be consistent with thrust-faulting earthquakes occurring deeper than the observed normal-faulting earthquakes within the downgoing plate.

4.5 The New Hebrides

Seismicity along the outer rise and trench slope of the New Hebrides is dominated by normal-faulting earthquakes (Fig. 8). Earthquakes in the downgoing plate are more frequent at the southern end of the subduction zone, where two large magnitude (M_W 7.6, 7.1) normal-faulting events, and their associated aftershock sequences have occurred. One of these events (the M_W 7.1 at −22.25°N, 169.75°E, purple mechanism on Fig. 8) has a complex source, and did not yield a robust solution to the simple modelling techniques employed in this study. Again, it is notable that the strike of the normal faulting earthquakes appears to track the local orientation of the trench around a bend. Extensional activity appears to reach down to $\sim$29 km. The gCMT catalogue provides evidence of sparse compressional seismicity, with reported depths as great as 68 km, but none of these earthquakes are large enough for their depths to be accurately determined with the techniques employed here. A single shallow compressional earthquake has occurred at the northern end of the subduction zone. Relatively high-angle nodal planes, and a location slightly seawards of the trench suggest that this occurred in the outer rise, but given the shallow depth and the proximity to the trench, even a slight mislocation could result in a hypocentre more consistent with activity on the interface or within the overriding plate. Seismicity around −15.75 ± 1.5°N is complicated by the subduction of the thickened regions of oceanic crust associated with the D'Entrecasteaux Ridge.

4.6 The Samoa-Tonga-Kermadec subduction zone

The Samoa-Tonga-Kermadec subduction zone (Fig. 9) is notable for the high levels of outer-rise seismicity it experiences, particularly compressional outer-rise seismicity. For the rest of this study, the

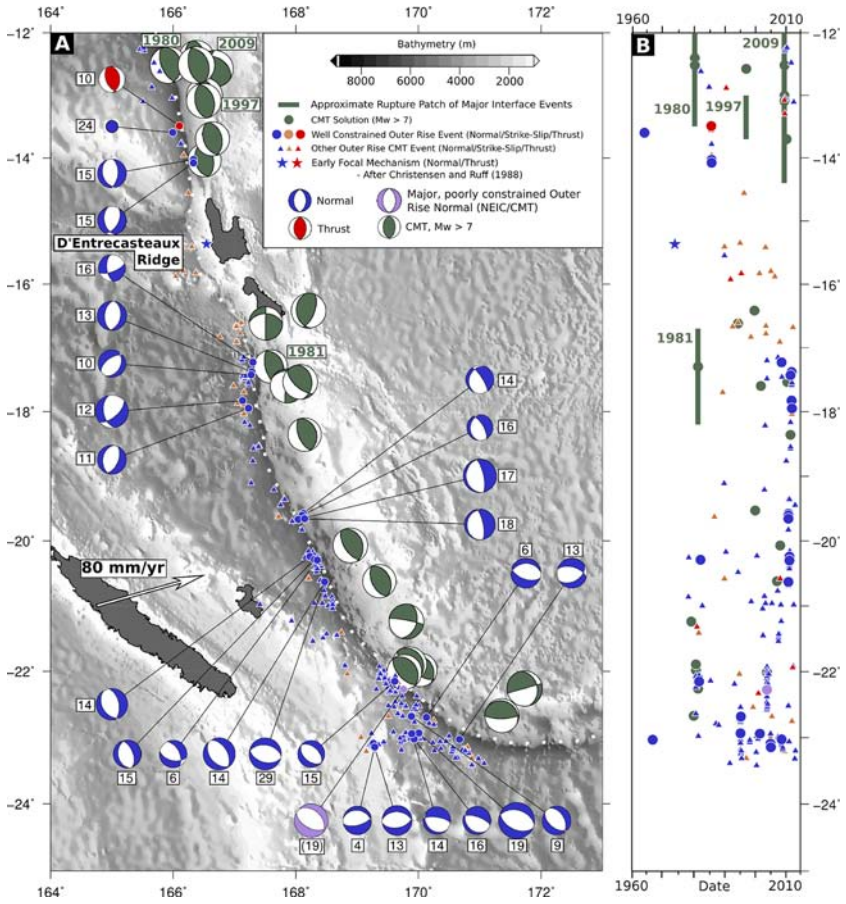

Figure 8. Outer-rise seismicity along the New Hebrides arc. (a) Seismicity and focal mechanisms. Seismicity at the southern end of the arc is dominated by two major outer-rise normal faulting events, and M_W 7.6 on 1995 May 16 and an M_W 7.1 on 2004 January 3. Earthquakes are included from Chapple & Forsyth (1979); Chinn & Isacks (1983); Liu & M^{c}Nally (1993). (b) Time versus latitude plot.

Tonga-Kermadec subduction zone is split into three sections—a northern section, north of 20°S, a central section from 20°S to 27°S, and a southern section south of 27°S (dashed orange bars, Fig. 9).

In 2009, the Samoa earthquake sequence struck the northernmost end of the Tonga trench (Lay *et al.* 2010). Here, a major (M_W 8.0) outer-rise normal-faulting earthquake occurred, and was followed by a pair of large (M_W 7.8) thrust-faulting earthquakes on the adjacent subduction interface, ∼50 and ∼90 s after the initial normal-faulting earthquake. The outer-rise main shock rupture extended from the surface to 24–30 km (Lay *et al.* 2010) with extensional aftershocks extending over a similar depth range (Fig. 9). The stress state in the region of 2009 Samoa sequence is probably complicated by the rapid change in trench orientation (and hence orientation of the bending stresses) at the north end of the subduction zone.

South of the bend in subduction zone orientation, numerous shallow normal-faulting and deeper thrust-faulting earthquakes have occurred, spread throughout the instrumental period, in a region with little recorded large-magnitude interface activity (Fig. 9b). While the orientations of the nodal planes of both the normal- and thrust-faulting earthquakes close to the trench are uniformly sub-parallel to the orientation of the trench, the compressional earthquakes further seawards from the trench show a range of nodal-plane strikes, potentially related to variable structure within the incoming plate.

South of 19°S, in the central section of the subduction zone as marked on Fig. 9, there is a concentration of compressional seismicity between 30 and 47 km, with shallower tensional earthquakes at 5–23 km. Subduction of the Louisville ridge at 26°S is marked by the occurrence of a single large normal-faulting event (Eissler & Kanamori 1982). Given the centroid depth and magnitude of this earthquake (20 km, for a M_W 7.2 event), standard scaling relationships potentially indicate relatively deep failure of the plate in tension at this point, perhaps down to ∼30 km (Eissler & Kanamori 1982).

South of the Louisville ridge, outer-rise earthquake activity is concentrated in the region of the 2011 Kermadec doublet (Todd & Lay 2013). Here, a shallow normal faulting earthquake (rupture from 0 to 25 km depth, Todd & Lay 2013) broke the upper part of the plate, accompanied by extensional aftershocks over the same depth range, and was followed 5 months later by a deeper thrust event (centroid at 39 km, rupture from ∼30 to 52 km depth).

A number of major ($M_W \geq 7$) outer-rise earthquakes have occurred along the Tonga-Kermadec subduction zone that are either too old for digital data to be available, or too large, and the waveforms too complex, to yield robust solutions using the techniques employed in this study (pale mechanisms, Fig. 9). Consideration of NEIC centroid depth shows these to be broadly consistent with the overall depths of normal-faulting and thrust-faulting from well-constrained events in the outer rise along the subduction zone.

Further south of the area shown (36–38°S), limited focal mechanisms with well-determined depths east of the Hikurangi trough indicate shallow extension, with the gCMT catalogue providing some evidence for deeper compression (Webb & Anderson 1998).

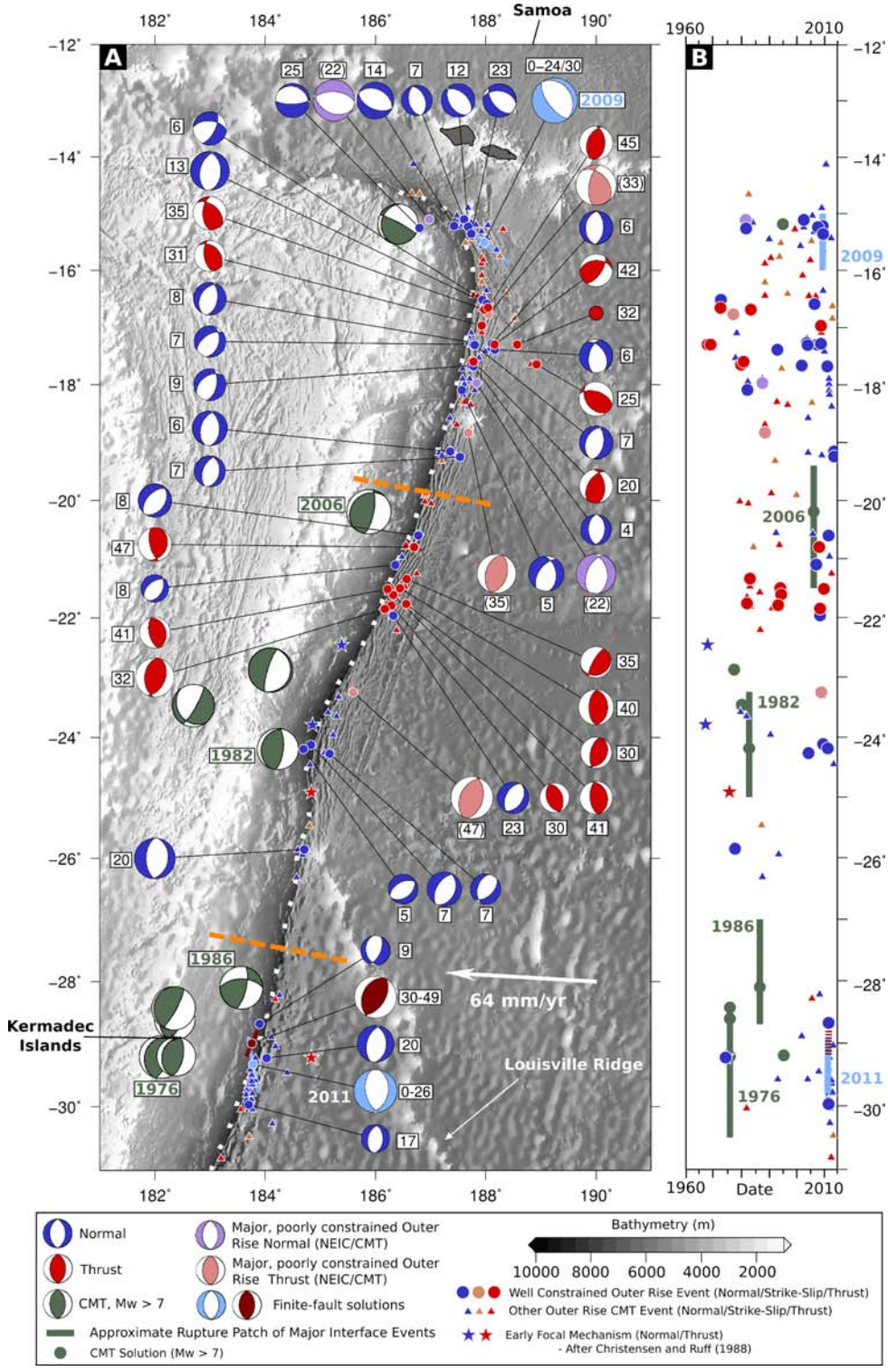

Figure 9. Outer-rise seismicity along the Samoa-Tonga-Kermadec subduction zone. (a) Seismicity and focal mechanisms. Light blue mechanism and bar represent the mechanism and rupture extent of the finite fault model of Lay *et al.* (2010) for the outer-rise component of the 2009 Samoa doublet, and the finite fault model of Todd & Lay (2013) for the extensional part of the 2011 Kermadec doublet. Dark red mechanism and bar are the compressional part of this doublet, from the same study. Depth extent of finite fault ruptures is based on the depth over which the majority of resolvable slip occurs. Earthquakes are included from Chapple & Forsyth (1979); Chen & Forsyth (1979); Eissler & Kanamori (1982); Forsyth (1982); Liu & McNally (1993). Orange dashed lines indicate the separation points between northern, central and southern sections of the subduction zone, as referred to in the text and Table 1. (b) Time versus latitude plot.

Triggering of interface activity by outer-rise events has been reported in at least two places along this subduction zone—immediately following the Samoa outer-rise event (Lay *et al.* 2010), and following both extensional and compressional earthquakes in the 2011 Kermadec doublet (Todd & Lay 2013).

4.7 The Chilean subduction zone

Fig. 10 summarizes outer-rise seismicity along the Chilean subduction zone. Extensional seismicity is seen along the length of the subduction zone, concentrated in the region seaward of the 1960 M_W 9.5 Valdivia earthquake, and seawards of the 2010 Maule earthquake (Fig. 10b). The deepest normal-faulting earthquake along the margin is 23 km below the seabed. The depth of the largest outer-rise aftershock of the 2010 M_W 8.8 Maule earthquake, a M_W 7.4 normal-faulting event, is poorly constrained due to complexities in the source. The NEIC depth of 20 km suggests it is consistent with other normal-faulting earthquakes along the Chilean subduction zone.

Three compressional events with well-constrained source depths have occurred along the margin. Of these, the largest is the M_W 7.2 1981 October earthquake (Honda & Kawakatsu 1990; Tichelaar *et al.* 1992). Detailed study of this event indicates that it had a centroid between 28 and 32 km. Rupture may have extended as shallow as 17 km and as deep as 43 km, but this is poorly constrained (Tichelaar *et al.* 1992).

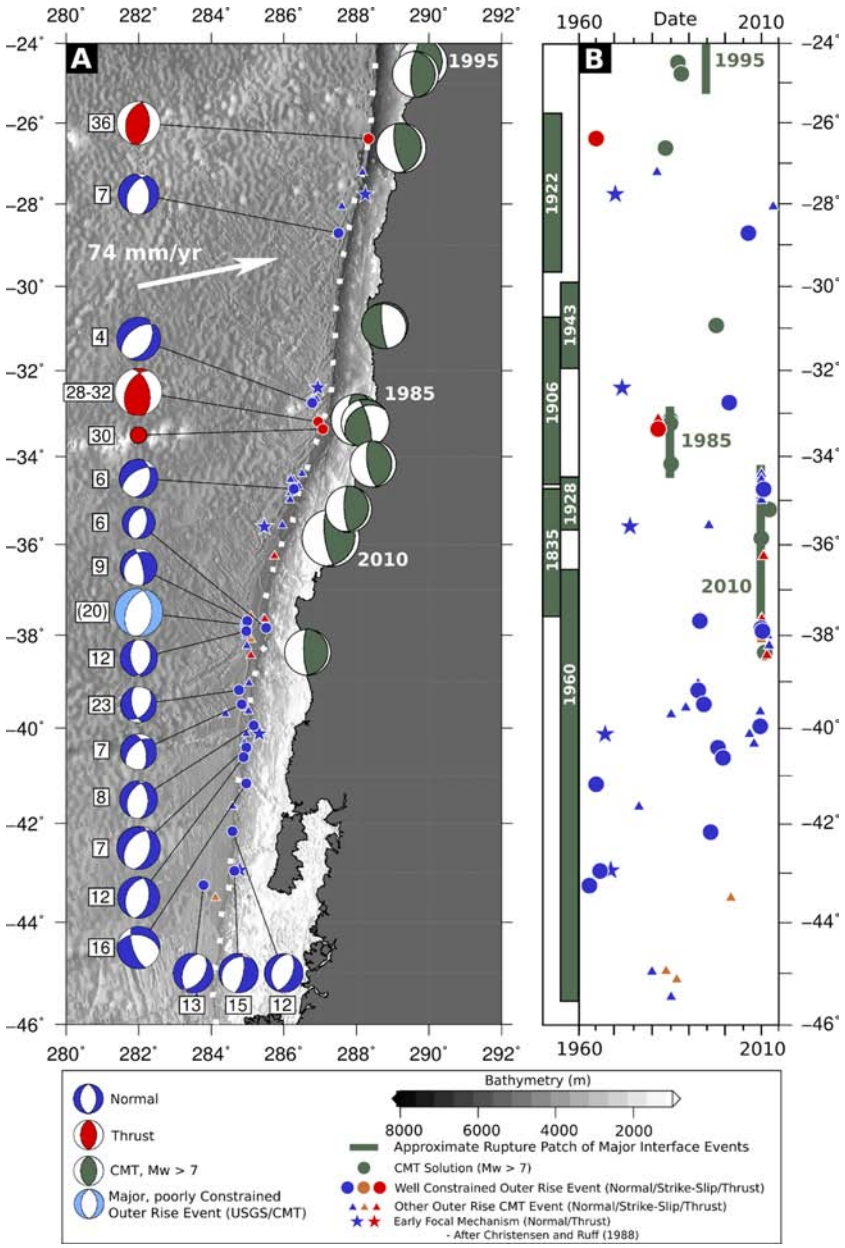

Figure 10. Outer-rise seismicity along the Chilean subduction zone. (a) Seismicity and focal mechanisms. A range of centroid depths are shown for the M_W 7.1 1981 compressional earthquake (−33.195°N −73.057°E), based on modelling by Tichelaar *et al.* (1992). The red dot is for an earthquake where the mechanism is constrained to being compressional through first motions, but the exact focal mechanism is poorly constrained. Earthquakes are included from Chinn & Isacks (1983); Korrat & Madariaga (1986). (b) Time versus latitude plot.

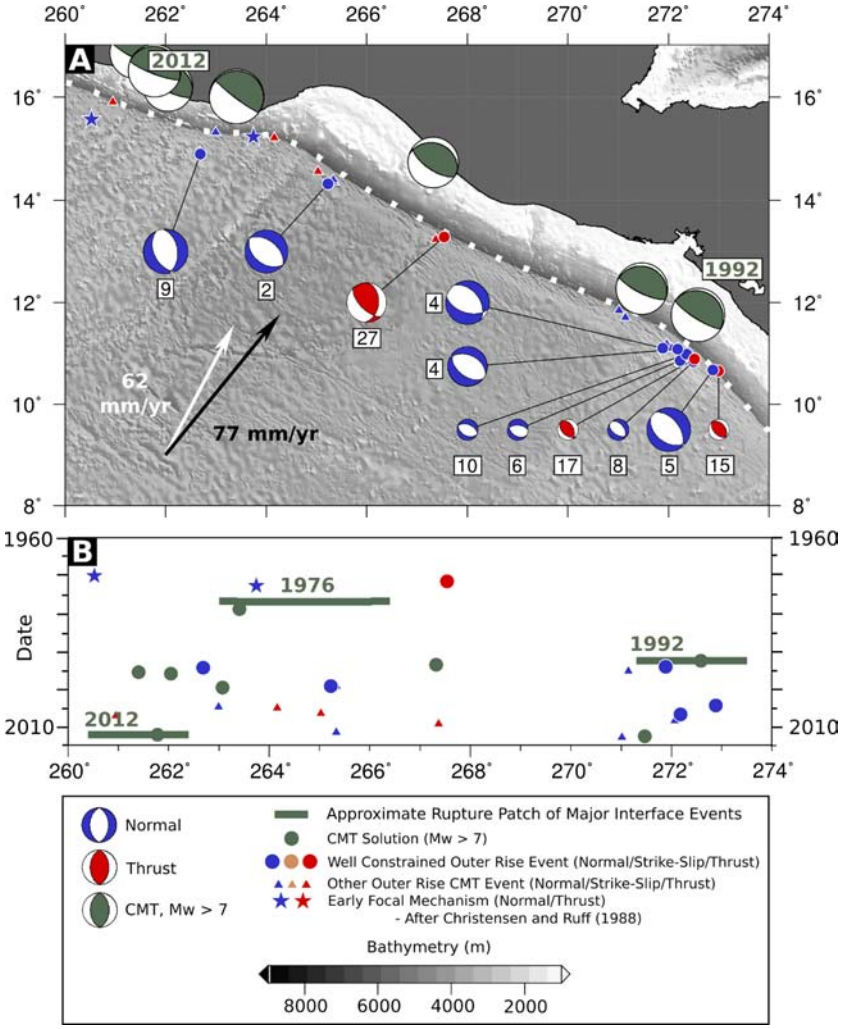

Figure 11. Outer-rise seismicity along the Middle American subduction zone. (a) Seismicity and focal mechanisms. Included are those focal mechanisms derived from a local OBS survey (small mechanisms; Lefeldt *et al.* 2009). Earthquakes are included from Chapple & Forsyth (1979). (b) Time versus longitude plot.

4.8 The Middle America trench

During the instrumental period, the Middle America trench has experienced relatively little outer-rise seismicity (Fig. 11). Five normal-faulting and one thrust-faulting earthquake have well-constrained depths from teleseismic studies, with a number of additional normal-faulting earthquakes reported (gCMT catalogue, Christensen & Ruff 1983). All five normal-faulting earthquakes are shallow ($\leq$10 km), and a single thrust-faulting earthquake much deeper (>26 km). Conclusions from teleseismic analyses are supported by the local study of Lefeldt *et al.* (2009). Five focal mechanisms were determined in the course of their study (small focal mechanisms, Fig. 11), which between them bracket the transition from extension to compression as being between 10 and 15 km below the seafloor.

4.9 The Philippines subduction zone

The Philippine trench has a history of small, infrequent outer-rise normal-faulting earthquakes throughout the instrumental period (Fig. 12). Little compressional activity was observed prior to a sequence of earthquakes starting with a M_W 7.6 compressional earthquake on 2012 August 31 (Ye *et al.* 2012). This sequence, starting with the major deep thrust event rupturing between ~25 and 55 km (Ye *et al.* 2012), continued with a series of smaller magnitude normal faulting earthquakes at much shallower depth.

4.10 Sumba

Seismicity at the eastern end of the Sunda arc, at Sumba, is dominated by the M_W 8.3 1977 Sumba outer-rise normal-faulting earthquake (Lynnes & Lay 1988), and its associated aftershock sequence (Fig. 13). The Sumba earthquake, the second largest recorded normal-faulting earthquake in the world after the 1933 Sanriku event, is believed to have ruptured down through the oceanic lithosphere to depths of at least 30 km, and maybe as deep as 50 km (Lynnes & Lay 1988). The aftershock sequence, which continues in the region to the present day, similarly covers a depth range from 0 to 30 km (Fitch *et al.* 1981; Spence 1986, this study). No evidence for compressional faulting is found along the eastern end of the Sunda arc, and the entire thicknesses of the observed seismogenic layer of the downgoing plate appears to be in down-dip tension.

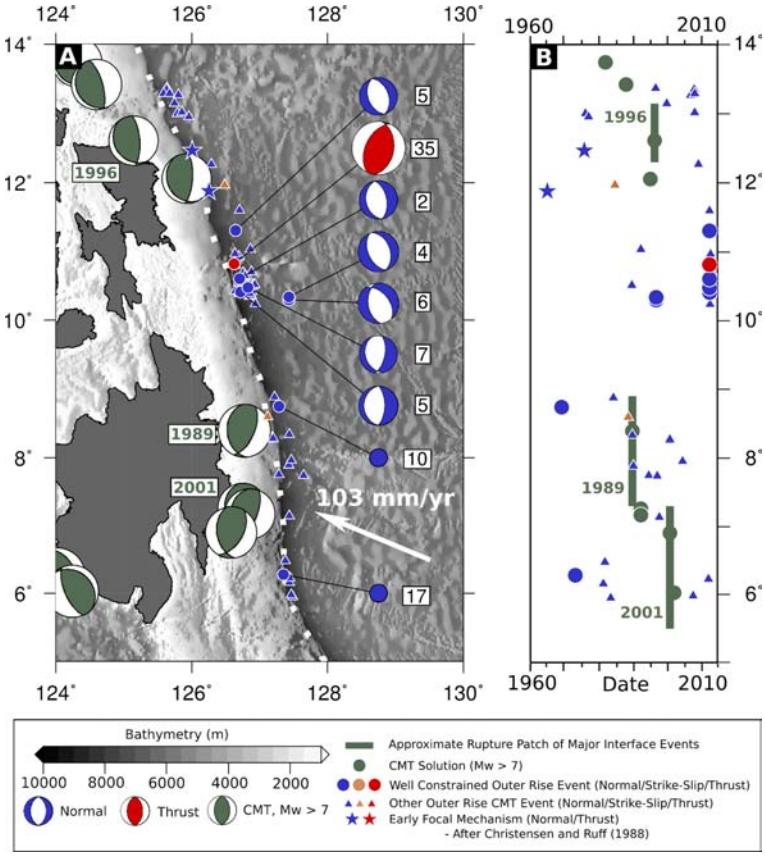

Figure 12. Outer-rise seismicity east of the Philippines. (a) Seismicity and focal mechanisms. Earthquakes are included from Chapple & Forsyth (1979); Seno & Yamanaka (1996). (b) Time versus latitude plot.

4.11 Sumatra

Signficant outer-rise seismicity has been observed along the Sunda arc west of Sumatra, seawards of the rupture patches of the 2004 Aceh-Andaman and 2005 Nias earthquakes (e.g. Dewey *et al.* 2007; Pesicek *et al.* 2010), with shallow thrust earthquakes in the near-trench environment. Seismicity in the oceanic plate along this subduction zone represents a more complex pattern of deformation than that seen at the other regions discussed here, and warrants a more detailed assessment of the wider distribution of seismicity within the downgoing lithosphere of the Indian Ocean (Craig & Copley, in preparation).

4.12 Summary of observations

A number of important trends stand out from our observations:

(i) The occurrence of both thrust- and normal-faulting earthquakes, and their tendency to align with the strike of the trench in many cases (e.g. Tonga, New Hebrides), indicates the importance of bending stresses in generating outer-rise earthquakes.

(ii) Observed moment release related to outer-rise seismcity can be highly variable along strike of subduction zones.

(iii) Not all outer-rise regions show both normal- and thrust-faulting earthquake activity, with some only failing in normal-faulting earthquakes (Sumba, western Aleutians), and others failing only in thrust-faulting earthquakes (Nankai).

(iv) The cases where both normal- and thrust-faulting earthquakes occur, they are separated in depth, with normal-faulting earthquakes occurring at shallower depth.

(v) The outer rise can, under certain circumstances, remain in trench-normal compression at depth and capable of brittle failure in earthquakes, following major seismic activity on the adjacent subduction interface (as seen seaward of the Kurils, and the east coast of Honshu).

We now further discuss these observations, and their implications for the mechanics and rheology of oceanic lithosphere.

5 THERMAL CONTROLS ON OCEANIC SEISMICITY

The depth extent of seismicity in the oceans depends on the thermal structure of the lithosphere, and hence on its age (Wiens & Stein 1983; McKenzie *et al.* 2005). Oceanic seismicity away from active mid-ocean ridges and from subduction zones is relatively sparse. As a result, outer-rise earthquakes represent an important part of the data set of oceanic seismicity which can be used to investigate the thermal control on seismogenic behaviour. Comparisons of seismicity to early models for plate thermal structure (e.g. Parsons & Sclater 1977) indicated that the deepest extent of oceanic seismicity approximately followed the depth of the 750 °C isotherm. However, more recent thermal models, taking into account the temperature dependence of thermal parameters within the mantle, lowered this threshold temperature to ∼600 °C (Denlinger 1992; McKenzie *et al.* 2005). The addition of new earthquake depths from this study to the existing data set for oceanic and outer-rise earthquakes continues to corroborate this temperature limit (Fig. 14). Earthquakes from regions where the age of the oceanic lithosphere is poorly

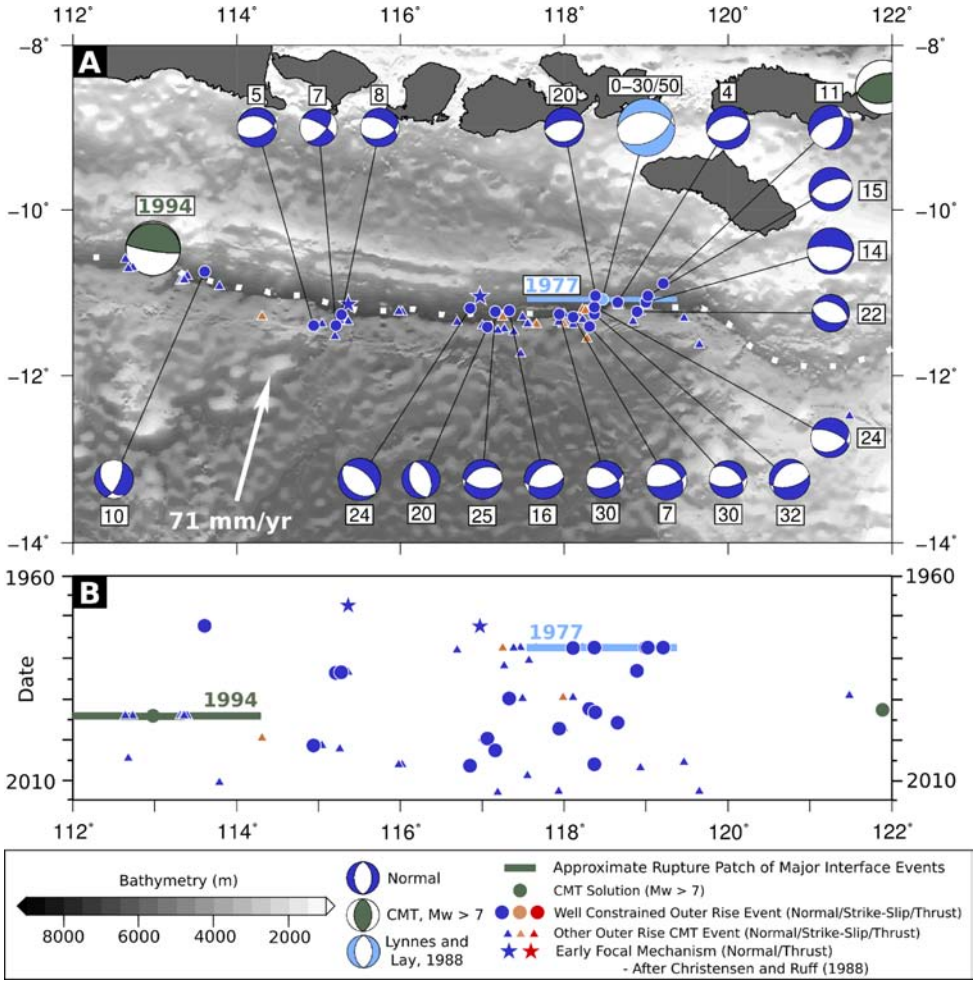

Figure 13. Outer-rise seismicity near Sumba. (a) Seismicity and focal mechanisms. The light blue mechanism and bar represents the focal mechanism and probable along-strike extent of the M_W 8.3 1977 Sumba main shock (Lynnes & Lay 1988). Earthquakes are included from Fitch *et al.* (1981); Forsyth (1982); Seno & Yamanaka (1996). (b) Time versus longitude plot.

constrained (e.g. seawards of the Hellenic arc) are excluded. In Fig. 14, seismicity is overlain on thermal structure, calculated for a 106-km thick plate using the techniques and parameters of McKenzie *et al.* (2005). This is a 1-D, time-dependent model with temperature-dependent thermal parameters, and accounts for isentropic melting of the mantle beneath the ridge. The plate thickness is based on the fitting the subsidence of oceanic lithosphere as a function of age, determined by Crosby *et al.* (2006). As Fig. 14 demonstrates, all oceanic earthquakes with well-constrained depths occurred at, or within error of, a temperature of $\lesssim$600 °C.

In the previous compilations of McKenzie *et al.* (2005) and Jackson *et al.* (2008), a single earthquake broke this trend—an M_W 6.4 earthquake from the Chilean outer rise from 1964 August 18. The initial modelling of this earthquake, by Chinn & Isacks (1983) estimated the depth as 48 km, 41 km below the seafloor, and beneath the predicted 600 °C isotherm. However, their study was limited to using *P*-waves only, and used a source-time function of 1 s duration—unusually short for an earthquake of this magnitude. Remodelling of the earthquake, incorporating *SH*-waves, and inverting for the source-time function, results in a depth of 36 km below the seafloor, with a longer source-time function duration of 4 s (Fig. S2). The new depth is used in plotting Fig. 14, shown by the orange circle, and was included on Fig. 10. This result emphasises the point made in Section 3.1 regarding the difficulties of precise determination of depths for underwater earthquakes if only limited data are available—particularly if shear-wave data are not used.

The age-dependence of seismogenic thickness, and the seismic-aseismic transition at ∼600 °C, observed from such global comparisons of oceanic seismicity and plate thermal structure match remarkably well with both seismological and experimental studies modelling the temperature control on seismicity along oceanic transform faults (Abercrombie & Ekstrom 2001; Boettcher *et al.* 2007), where a limit of 600 °C is also determined. Similarly, the results of local earthquake studies in oceanic lithosphere, along with region-specific thermal models, in which the initial mid-ocean ridge thermal structure is calibrated to fit the thickness of oceanic crust observed, fit the same thermal limit (Tilmann *et al.* 2008; Lefeldt *et al.* 2009).

6 DEPTH EXTENT OF NORMAL AND THRUST FAULTING

A simple view of the deformation of a bending plate suggests that thrust faulting should be confined to depths deeper than normal faulting. Fig. 15(a) shows the depth extent of seismicity in each of the regions presented in this paper. In each case, normal-faulting earthquakes are indicated by blue T-axes, thrust-faulting earthquakes by red T-axes. In all regions, a clear separation is seen

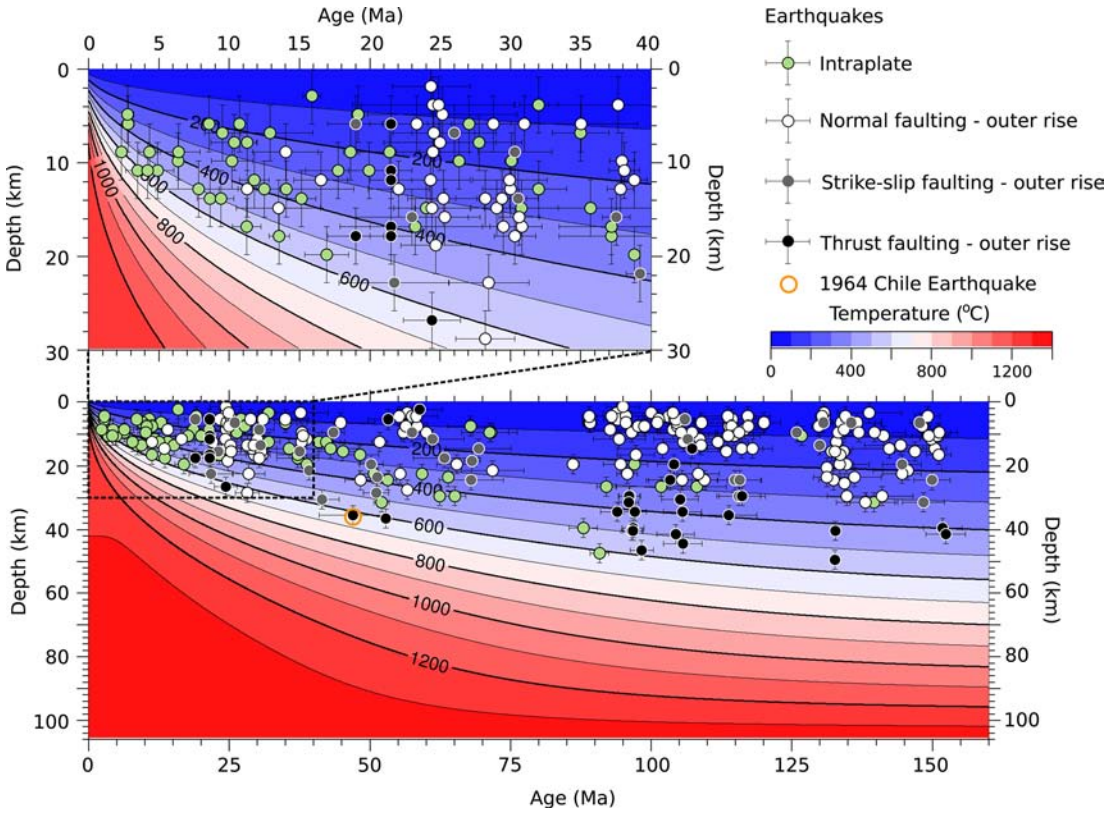

Figure 14. The depth extent of outer-rise seismicity with plate age and thermal structure. This figure is an update to that included in Jackson *et al.* (2008), from which the depths and locations of intraplate oceanic earthquakes away from outer rises are taken. Earthquake depths are plotted against plate age from Muller *et al.* (2008). Age uncertainties are based on the plate age uncertainties of Muller *et al.* (2008). Representative earthquake depth errors are shown, and based on the routine technical errors, as discussed in the text. The thermal structure of the plate is calculated using the method and parameters of McKenzie *et al.* (2005), with a plate thickness of 106 km, and a mantle potential temperature of 1315 °C. The initial thermal structure of beneath the mid-ocean ridge is calculated accounting for isentropic melting of the mantle. The 1964 Chile event, discussed in the text, is indicated by the orange circle.

between shallow normal-faulting earthquakes and deeper thrust-faulting earthquakes. The thickness of the separating region varies, but can be as small as ∼2 km (east of Honshu). A number of regions (the Aleutian arc, and Sumba) show only normal faulting, with no deeper earthquakes indicating compression.

Seismicity in Fig. 14 is limited to depths shallower than, or within error of, the expected depth of the 600 °C isotherm, shown by the yellow bars on Fig. 15, and based on the plate-cooling models of McKenzie *et al.* (2005). In a number of regions, seismicity cuts off at depths significantly shallower than the expected depth of the 600 °C isotherm (Sumba, the Aleutian arc, Samoa). This may be a result of the length of the observation period relative to the duration of the seismic cycle. However, there may be significant regions at the base of the the seismogenic plate where the stresses are low enough to be supported elastically, rather than resulting in brittle failure in earthquakes, and this may be the reason for the lack of deep compressional seismicity along the Aleutians and at Sumba.

7 TEMPORAL VARIATIONS IN THE STRESS STATE OF THE OUTER RISE

Variations in the magnitude of stress transmitted across the subduction interface over the seismic cycle might be expected to result in a variation in the stress state at the outer rise through time. It is well documented that seismic activity on the subduction interface can trigger subsequent activity in the adjacent plate, and such behaviour is widespread (e.g. Lay *et al.* 2011). Most recent megathrust earthquakes have been followed by widespread extensional outer-rise seismicity (see Figs 3, 4, 10). However, nowhere can the depth to deepest horizontal extension, or the depth to shallowest horizontal compression, be observed to have varied significantly in time following motion on the interface. Nowhere have normal-faulting earthquakes occurring after an interface event been observed at depths marked by thrust-faulting earthquakes prior to motion on the adjacent megathrust. Indeed, in all regions clear separation is seen at all times between extension and compression (Fig. 15). Given the sparse nature of outer-rise seismicity, it cannot be ruled out that a temporal switch in the stress state from extension to compression at a given depth does occur, but increasing evidence suggests that any depth range over which this does occur is small.

If motion on the interface does not significantly affect the depth of the transition from normal-faulting earthquakes to thrust-faulting earthquakes, or the thickness of the region over which this transition takes place, then it can be inferred that the modulation of stress transferred across the interface over the seismic cycle is insignificant in determining the depth of transition from horizontal extension to horizontal compression within the downgoing plate when compared to the imposed stresses over timescales longer than the seismic cycle—that is, those arising from the overall plate-driving forces. Outer-rise aftershocks therefore presumably represent faults already close to failure that the small stress change due to the megathrust event can bring to the point of failure.

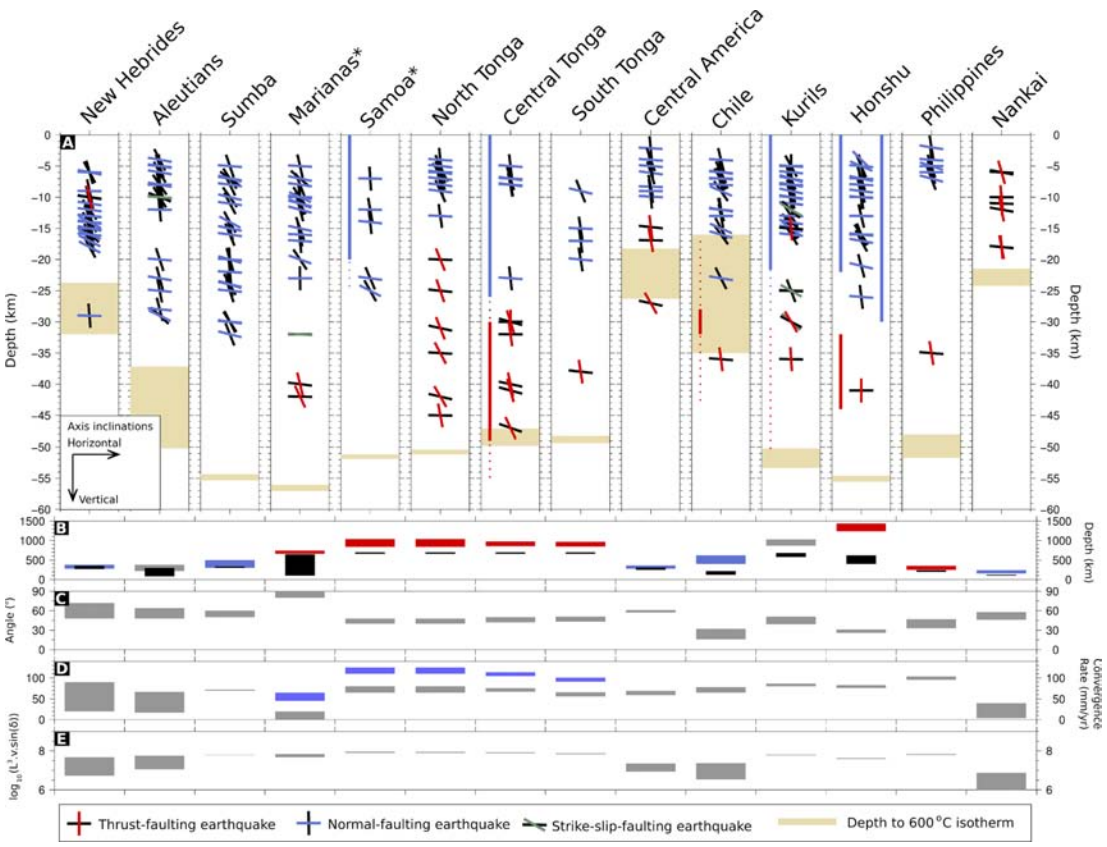

Figure 15. Depth-dependent deformation in the outer rise. (a) Earthquake P- (black) and T- (coloured) axes inclinations for earthquakes with well-determined depths. For thrust-faulting earthquakes, T axes are coloured red. For normal-faulting earthquakes, T axes are coloured blue, for strike-slip earthquakes, T axes are coloured green. Yellow boxes indicate the depth range over which the 600 °C isotherm is expected to occur, based on the plate age (Muller *et al.* 2008) and the thermal models of McKenzie *et al.* (2005). The range shown results from the range in plate age along the region considered. Coloured bars to either side of earthquake P/T axes represent additional constraints from local seismic surveys (Honshu) and from finite fault models, as discussed in the text (Samoa, Kurils, Chile). Bars are dashed when the depth extent is uncertain. The Aleutians column excludes the mechanisms from Fig. 2(b), based on their distance from the trench. Regions with large along-strike trench curvature are marked by an asterisk. (b) Downdip slab length, coloured by downdip deformation style (red = compression, blue = extension, grey = complex), and vertical distance to deepest earthquake (black). Where a range is shown, it indicates variations along the strike on the subduction zone in the region considered. (c) Slab dip. (d) Convergence rate (grey) including backarc extension if present Jarrard (blue—after 1986). (e) Proxy for the magnitude of slab pull, as discussed in the text.

It has also been suggested that the buildup and release of stress on the subduction interface modulates the temporal occurrence of seismicity in the outer rise, in addition to the presence of outer-rise aftershocks (Christensen & Ruff 1983, 1988; Lay *et al.* 1989). However, in a number of cases, the simple expectation of compression prior to an interface event, followed by extension afterwards, does not hold. Major compressional earthquakes within the downgoing plate have been seen following the 2011 Tohoku earthquake off Japan (Fig. 4) and following the 2006 earthquake in the Kurils (Fig. 3). Small-scale thrust-faulting earthquakes in the downgoing plate followed the 2010 Maule earthquake offshore Chile (Fig. 10). Along the Tonga-Kermadec subduction zone, both extensional and compressional activity within the downgoing plate are seen both before and after interface activity, and the 2009 Samoa doublet involved an interface event triggered by an extensional outer-rise earthquake (Lay *et al.* 2010), although we note that the triggered interface event is laterally offset from the triggering outer-rise earthquake. A quantitative assessment of the global time variation in the seismicity of the outer rise is beyond the scope of this study. However, the qualitative observations from Figs 2 to 11 suggest that while triggering is prevalent, time-varying stress transfer across the interface typically has little influence on the depth extent of outer-rise earthquakes. A small number of observations indicate that failure in both the compressional and extensional parts of the bending plate remains possible throughout the interface seismic cycle, although it should also be noted that the role that outer-rise events may have on triggering other events in the conjugate part of the bending plate remains uncertain. The dominant influence of interface activity therefore appears to be in triggering the failure of outer-rise faults already stressed close of the point of failure.

8 CONTROLS ON THE DEPTH EXTENT OF EXTENSION AND COMPRESSION AT THE OUTER RISE

Fig. 14 shows a first-order separation of shallow extensional (white) and deeper compressional (black) outer-rise seismicity. Fig. 15 splits the data set into individual regions, showing the inclination of P- and T-axes for each area, to examine the controls on the depth of the transition from extension to compression.

The depth of the transition from normal faulting to thrust faulting (if this occurs) is expected to be controlled by four main factors: the magnitude of the bending moment, the magnitude of any in-plane

stresses within the plate (arising from both forces transmitted along the plate from the descending slab, and forces exerted from seaward of the trench), the rheology of the plate, and the subduction interface stress. In cases where the overall in-plane force is extensional, the depth to the transition from horizontal extension to compression will be deeper than half way through the stress-supporting section of the plate (assuming that the stress required to break the plate in earthquakes is either independent of, or increases with, depth). For compression to extend into the upper sections of the plate, the in-plane force must be compressive. Similarly, if stresses are mainly supported in the upper brittle part of the plate, rather than the deeper viscous part, then for the entire seismogenic plate to be undergoing brittle failure in extension, the in-plane force must be extensional.

Ridge push will have an influence on the stress state at the outer rise. This force can only be compressional, with its magnitude depending on the geometry and age distribution of the oceanic plate seaward of the subduction zone, and the age of the plate at the trench. Estimates of ridge-push suggest it is $\lesssim 3 \times 10^{12}$ N m^{-1} (e.g. Parsons & Richter 1980). The majority of subduction zones considered here have oceanic lithosphere at the trench older than 75 Ma, the age at which the age-depth curve for the oceans flattens out (Crosby *et al.* 2006), and so ridge push is likely to vary little between them. The exceptions to this are the subduction zones along Central/South America, the New Hebrides and the Nankai trough. Thermal contraction of the cooling oceanic plate may also affect the stress state of the incoming plate seaward of the trench, and, as with ridge push, can only have a compressional influence on the outer-rise stress state. Similarly, any dynamic topography of the oceanic plate, and the resultant contrasts in gravitational potential energy, will influence the in-plane stresses on the incoming plate. Dynamic topography will be variable, and is particularly hard to assess (e.g. Winterbourne *et al.* 2009). However, stresses resulting from dynamic topography are rarely sufficient alone to cause seismicity within oceanic plates, and so are not likely to be a dominant influence on the outer-rise stress state.

The along-strike curvature of the trench will also influence the stress state at the outer rise (Mahadevan *et al.* 2010). These effects are minimized in the analysis that follows by focussing on subduction zones with little along-strike curvature. Hence, the effects of along-strike plate curvature are assumed to be negligible in all cases except for Samoa and the Marianas arc (marked by an asterisk on Fig. 15), where the trench rapidly changes strike, and stresses acting along-strike may be significant.

If slab-pull contributes significantly to driving plate motions (Forsyth & Uyeda 1975), it is expected that the in-plane forces in regions with significant lengths of attached slab will be dominated by the effect of forces derived from the plate downdip of the trench. In the cases where the slab has not yet reached depths close to the mid-mantle discontinuity at ∼660 km, the slab is typically in overall downdip tension, as indicated by intermediate and deep earthquake focal mechanisms (Isacks & Molnar 1971). Those slabs that have reached deep into the upper mantle, close to the mid-mantle discontinuity, typically experience sufficient resistive force to go into downdip compression. In cases where the downdip compression within the slab reaches to shallow depths, the in-plane force applied to the outer rise is also likely to be compressional.

Variations in the depth of the transition from horizontal extension to compression beneath the outer rise can be described as a function of six parameters: The magnitude of the slab pull, the magnitude of forces resisting the further penetration of the slab (essentially dependent on the magnitude of resistive tractions between the slab and surrounding mantle, and whether the deepest part of the slab has reached the 660 km discontinuity), the magnitude of the force transmitted across the subduction interface, the angle of slab dip (which influences the bending stresses), the combined effect of ridge push and thermal contraction of the plate, and the influence of dynamic topography seaward of the trench. The effect that these six parameters have on the deformation within the downgoing plate is schematically summarized in Fig. 16.

The previous section, Section 7, discussed the independence of the depth of normal- and thrust-faulting earthquakes relative to the timing of the interface seismic cycle, indicating that variations in the stress transmitted across the seismogenic part of the interface over the seismic cycle has little influence on the outer-rise stress state. This suggests that variations in the stress supported on the subduction interface are small when compared to the stresses arising from other factors that influence outer-rise seismicity, in agreement with other estimates for relatively low shear stresses supported on subduction interfaces (e.g. Wang *et al.* 1995; Lamb 2006).

Fig. 15(b–e) attempts to explore the various forces acting on the outer rise, by considering the geometry and deformation of the slab downdip of the subduction interface. Fig. 15(b) gives the depth to deepest earthquake (black bar) and the downdip slab length (based on the distribution of slab-related seismicity), coloured by downdip deformation mechanism within the slab (Isacks & Molnar 1971, gCMT catalogue). Figs 15(c) and (d) give the average slab dip and the convergence rate at the trench, respectively. Fig. 15(e) presents a proxy for the relative magnitude of density-derived slab pull (F_{SP}) acting along the plane of the plate, given by

$$F_{SP} = AL^3 v \sin(\delta), \tag{1}$$

where L is the thickness of the thermal plate, v is the subduction velocity, δ is the average slab dip, and A is a constant. The thermal plate thickness is taken as the depth to the 1300 °C isotherm in the standard plate model (Fig. 14), taken at the age of the incoming plate at the present day. This simple expression, based on those of M^{c}Kenzie (1969), does not account for variations in the age of the incoming plate, the subduction velocity through time, the effect of complexities in slab geometry, or the interaction of the slab with the 660 km discontinuity. However, it is sufficient to indicate the relative magnitude of the in-plane slab pull force at different subduction zones.

Two regions show extensional seismicity throughout the seismogenic part of the lithosphere seawards of the trench—the New Hebrides and the Aleutians. The lack of compressional seismicity at depth does not preclude the existence of a region near the base of the seismogenic plate from supporting compressional stresses, if the compressional stress is not sufficient to exceed the limit of the stress supportable on faults, or if our observation time is too short to capture the full range of seismicity. Both of these regions have relatively short (<500 km) slab lengths. The New Hebrides slab is in downdip extension, and the seismicity at the outer rise indicates that most, if not all, of the brittle part of the plate there is in tension, with normal faulting earthquakes extending down to depths consistent with the expected depth of the 600 °C isotherm. The western Aleutians similarly show only normal-faulting earthquakes in the outer rise, down through the majority of the plate, with no observed region of brittle failure in compression at depth. Observations of the deformation within the Aleutians slab are difficult to categorize into dominant downdip extension or compression. However, as with the New Hebrides, the slab beneath this region has not yet reached deep into the upper mantle, and hence the slab is likely to be in tension near the surface. These regions are therefore consistent with the influence of slab pull, without either the resistive effect of contact

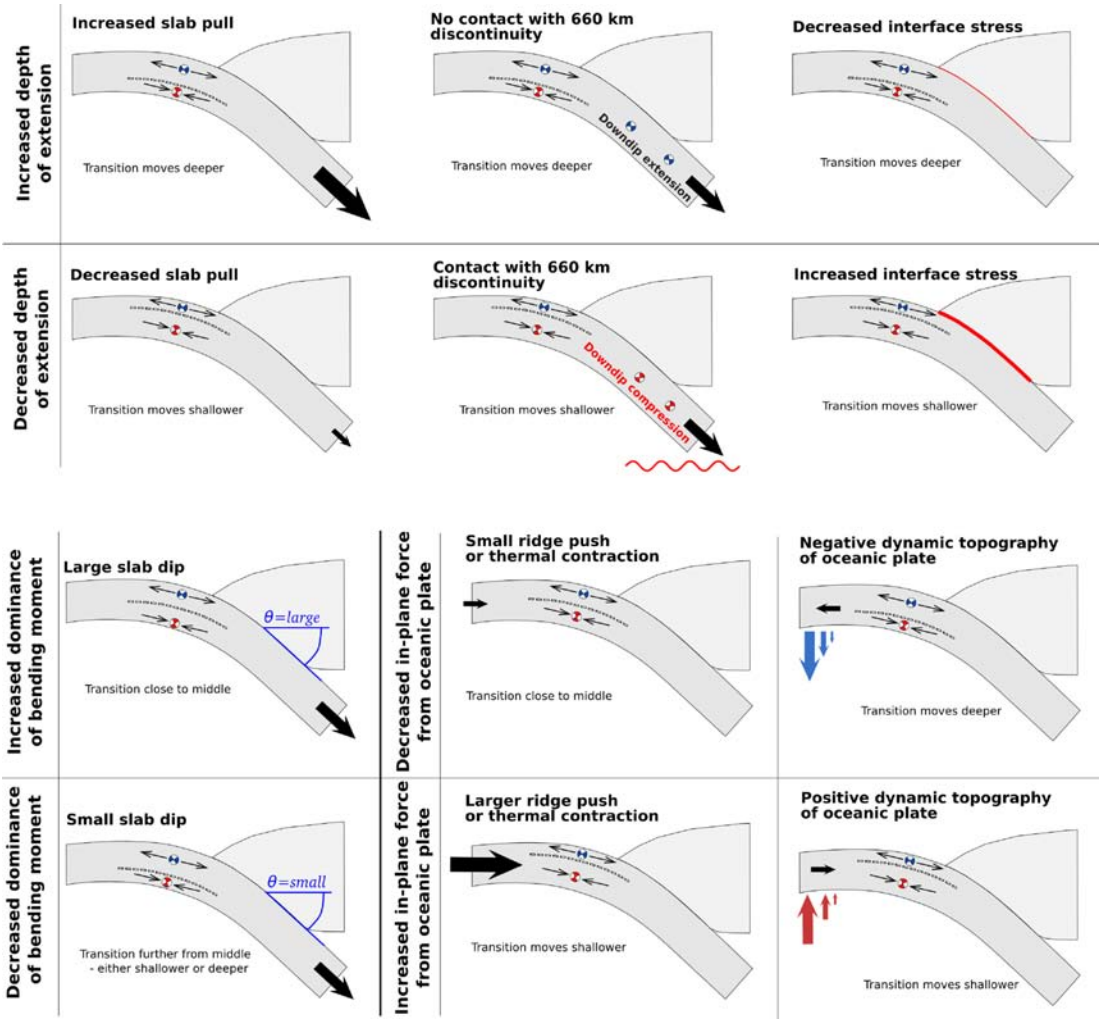

Figure 16. Schematic diagram for the factors influencing the depth of the transition from horizontal extension to horizontal compression beneath the outer rise. Slab pull, the interaction of the descending slab with the 660 km discontinuity (or increasing drag from the surround mantle), and variations in the interface stress influence both the bending moment and the in-plane stress. Increases in the angle of slab dip increases the dominance of the bending moment relative to the in-plane stress, and hence moves the depth of transition towards the middle of the mechanical plate from either an shallower or a deeper position. A decrease in slab dip enhances the influence of the in-plane stress, and hence moves the transition further from the middle of the mechanical plate, either deeper for an extensional in-plane stress, or shallower for a compressional in-plane stress. Increased plate age of the incoming plate leads to increases in the magnitude of ridge push and intraplate thermal contraction, increasing the in-plane compressional stress in the plate prior to bending. Dynamic topography of the oceanic plate seawards of the trench can result in either in-plane extension or compression prior to the application of the bending stresses.

with the 660 km discontinuity, or significant tractions with the surrounding mantle, putting the whole of the plate at the outer rise into extension.

Sumba also shows only extensional seismicity in the outer rise. However, there is a significant (∼20 km) thickness of plate beneath the deepest earthquake that is colder than ∼600 °C, and can potentially deform in earthquakes, but in which no seismicity has been observed. The Sunda slab beneath Sumba extends at a high dip angle down to the approximate depth of the 660 km discontinuity, and the downdip deformation within the slab is compressional. The high angle of slab dip into the mantle suggests high bending strain at the outer rise, which is likely to reflect the dominance of the bending moment, relative to the in-plane force, in influencing outer-rise deformation. At Sumba, we observe extensional seismicity over at least half of its seismogenic thickness seaward of the trench, in a situation where all the in-plane forces are expected to be compressional, and the only cause of extension should be the bending moment. This situation suggests either that the ductile part of the lithosphere is contributing significantly to the support of the stresses, or that the brittle part of the lithosphere can support greater stress at greater depth, equivalent to the yield stress increasing with depth.

As a result of the trench-parallel orientation of the P-axes for the two compressional earthquakes in the Marianas arc (Fig. 7), the interpretation of the stress state at depth along the Marianas outer rise is uncertain, and is probably complicated by the rapid change of strike in the trench along the subduction zone. Similarly, the stress state at the northern end of the Samoa-Tonga-Kermadec subduction zone, in the vicinity of the Samoa doublet, is likely to be complicated by the high degree of along-strike curvature in this region. These two regions cannot be investigated further with our 2-D approach to the mechanics of the plate.

Along the Nankai Trough, thrust-faulting earthquakes are seen throughout the seismogenic thickness of the downgoing plate beneath the trench. The effect of slab pull in this region, both in terms of the in-plane stresses and the bending moment, is likely to

be small (Fig. 15e), due to the short length of the slab (Fig. 15b) and the slow convergence rate (Fig. 15d). That the dominant force in this case is in the plane of the plate, rather than associated with the bending moment, is further shown by the distribution of deformation in the oceanic plate away from the trench, indicated by the formation of the compressional Zenisu ridge (Fig. 6). The observed dominance of compression probably results from the localized effects of proximity to the triple junction southeast of Honshu, and enhanced in-plane stresses transmitted across the plate contact resulting from the collision of the thickened crust of the Izu peninsula with the southern edge of Honshu (Chamot-Rooke & Le Pichon 1989).

In northern Tonga, and potentially east of Honshu, compressional seismicity is seen over halfway from the expected depth of the 600 °C isotherm to the surface, indicating that the plate is in significant in-plane compression. Both of these subduction zones have slabs reaching to the 660 km discontinuity, which are undergoing overall downdip compression along their entire length. The Kurils experiences compression over approximately half of the thickness of the seismogenic part of the plate. However, the deformation in the descending slab is complex, and cannot easily be attributed to an overall stress state. The southern sections of the Tonga-Kermadec subduction zone, and the Philippines, similarly show deep compressional earthquakes, indicating horizontal compression perhaps extending to halfway through the seismogenic part of the plate, matching with expectation for regions undergoing downdip compression in the rest of the slab. In these regions, we can therefore see the influence of forces resisting slab penetration on the deformation in the outer rise.

It is interesting to note that the depth extent of compressional earthquakes associated with the earthquakes in North Tonga on Fig. 15 reaches to significantly shallower depths than in the groups of earthquakes further south (Central Tonga—Fig. 15). This may suggest that the stress field can vary significantly on the scale of only a few hundred kilometres.

Central America and Chile both have compressional seismicity at depth within the seismogenic part of the plate, but have short slabs probably undergoing downdip extension, indicating that the influence of slab pull on the in-plane stress is likely to be tensional. However, both of these subduction zones have ramp-and-flat geometries, with the slab becoming subhorizontal at shallow depth beneath the arc, before then bending again to dip down into the mantle (e.g. Hayes *et al.* 2012). Note that the dip angle shown in Fig. 15(c) is an approximation to the overall slab dip, not the dip of the shallow slab. In such cases, the influence of slab pull on the outer rise is likely to be reduced, and hence the relative importance of compressional stresses transmitted across the subduction interface increased. In addition, the interpretation of slab seismicity as indicating downdip extension may be complicated by bending-related seismicity as the slab changes shape downdip of the trench (e.g. Vallée *et al.* 2003).

In summary, this section highlights the interplay between the factors controlling the depth of the transition from normal-faulting earthquakes to thrust-faulting earthquakes, as summarized in Fig. 16. Relative decreases in the depth to this transition result from increases in the in-plane downdip compressional stress, or decreases in downdip extensional stress. These can result from:

(i) A shorter downdip slab length, decreasing the magnitude of buoyancy-derived slab pull.

(ii) The contact of the leading edge of the slab with the 660 km discontinuity, resulting in a significant increase in the forces resisting further slab penetration in the mantle, or major tractions between the slab and the surrounding mantle, either of which would put the slab itself into downdip compression, rather than buoyancy-driven downdip extension.

(iii) Increased stresses transmitted across the main subduction interface, although this effect is probably minimal, as discussed.

(iv) Variations in the the age distribution of the incoming plate, influencing the magnitude of the compressional forces resulting from ridge push and thermal contraction.

(v) Dynamic topography of the incoming oceanic plate.

These parameters, influencing both the bending moment and in-plane stress, all result in changes to the depth of the transition from normal-faulting to thrust-faulting earthquakes relative to a hypothetical 'mid-point'. The elastic core would be positioned at this midpoint in the case where the in-plane stresses are zero, and deformation at the outer rise is the result of the plate bending only. The depth of the transition in this extreme case is controlled only by the rheology of the oceanic lithosphere, and the way in which it is able to support the bending stresses. Variations in the magnitude of slab pull, the interaction of the slab with the 660 km discontinuity, and the stress transmitted across the subduction interface result in changes in the in-plane stress, and hence can result in the transition from extension to compression moving either up or down relative to the 'mid-point'. Increases in the angle of the slab dip increase the total bending strain that must be accommodated. This can be viewed as increasing the size of the bending moment relative to the in-plane stress, and hence can only move the transition back towards the 'mid-point', and narrow the thickness of the core region around the 'mid-point' supporting stresses elastically. In summary, this section has demonstrated that the depth of the elastic core can be understood, at least in qualitative terms, based on the combination of a fairly small number of influences relating to the forces acting on the plates and its geometry.

9 SURFACE EXTENSION AND FAULTING AT THE OUTER RISE

Using earthquake depths to define a zero-strain depth within the plate, corresponding to the middle of the aseismic depth interval between normal faulting and thrust faulting, and under a simplifying assumption of constant curvature over the bending region, we can estimate the surface elongation rate (x') at the top of the plate as it bends into a subduction zone:

$$x'(z)|_{z=0} = \frac{v z_0}{r}, \tag{2}$$

where v is the convergence rate, z_0 the depth of zero-strain, and r the radius of curvature for the z_0 point.

The Japan trench east of Honshu has a zero-length-change depth at 29 ± 2 km (Fig. 15), an across-strike width of the bending region of ∼100 ± 20 km, an interface dip at the trench of 5°, and a convergence rate of ∼90 ± 5 mm yr^{-1}. Using the interface dip and width of the bending region to estimate the average curvature, the surface downdip elongation rate is estimated to be ∼2.3 ± 0.7 mm yr $^{-1}$. For the Kurils, similar calculations result in a surface elongation rate of ∼1.8 ± 0.6 mm yr^{-1}. Lay *et al.* (2009) estimate near-surface slip in the 2007 Kuril Islands extensional outer-rise event in excess of 13 m, on a fault dipping at 47°. Based on the estimated slip rate, such earthquakes might only be expected to occur every ∼5000 yr, although Lay *et al.* (2009) note that their slip estimates may be slight overestimates due to some of the model assumptions. In light of this repeat time, it is therefore no surprise that only one such earthquake

(which ruptured ∼200 km of the ∼1200 km subduction zone) has occurred in the last 50 yr for which instrumental records exist.

Similarly, and again under the assumption of constant curvature in the bending region, the total surface extension over the bending region, Δx, can be estimated using

$$\Delta x = z_0 \theta, \tag{3}$$

where θ is the interface dip and z_0 the depth of zero-strain.

For the Japan trench east of Honshu, detailed bathymetric surveys analysing the distribution and characteristics of the outer-trench-slope faults have been conducted (Kobayashi *et al.* 1998). In this region, the faulting shows large vertical surface offsets (up to ∼400 m), along-strike fault lengths range up to ∼50 km, and the across-strike spacing is typically 5–10 km (Kobayashi *et al.* 1998). Adding up the total vertical fault throws along the three trench-perpendicular profiles presented by Kobayashi *et al.* (1998) for the Japan trench gives totals of $\lesssim$2000 m on each profile. Assuming fault dips of ∼45°, similar to the observed dip of seafloor escarpments (38°) and to the earthquake nodal plane dips, this value will be approximately equivalent to the total downdip surface extension accommodated on the major faults. Estimates for the surface extension for the Japan trench slope and outer rise from eq. (3), which suggest surface extension of >2500 m for the outer trench slope east of Honshu, are in sufficiently close agreement to the observed extension that the major faults can be assumed to be taking up the majority of the required extension. Additionally, the observed surface extension can be explained by bending, without the overall extension of the entire plate.

In some cases, erosion of the footwall and deposition in the hanging wall may reduce the bathymetric expression of outer-rise faults, reducing the estimated offset. However, seawards of the the Middle America trench, Ranero *et al.* (2003) determined fault offsets at the top of the basement beneath the sediment cover. These offsets add up to ∼1100 m, across the nearest 25 km of the incoming plate to the trench. While this survey only covers half of the extent of the bending region, it covers the region closest to the trench, likely to have the largest offsets. The estimated total extension for this region, using Equation 3, is ∼1.75 km, again consistent with the major faults that influence the surface bathymetry accommodating the majority of the extension.

The observed offsets of major outer-trench-slope faults are far larger than might be expected if the vertical displacement gradient along each fault is supported entirely elastically between the surface and the elastic core (where the fault displacements should reduce to zero). In the case of Japan, where the largest fault offsets have been observed, this would require the elastic support of ∼400 m of displacement (Kobayashi *et al.* 1998) over a region only 30 km wide (a strain of 0.013). Typical values for the elastic limit of rock ($<10^{-4}$) suggest that such displacement gradients cannot be supported only elastically over the depth range of upper plate seismicity, down to the elastic core. Hence, significant displacement gradients must be taken up anelastically, most likely by distributed internal faulting of the major fault-bounded blocks. Recent seismic imaging of the downgoing plate seaward of the trench east of Honshu, Japan, shows numerous closely spaced ($\leq$5 km) normal faults cutting the top of the plate, and dipping both into and away from the trench (Nakamura *et al.* 2013), supporting the idea of distributed small-scale faulting in small-magnitude earthquakes taking up deformation between the major high displacement faults. These smaller faults may serve to accommodate the high-displacement gradients seen on the major faults by allowing the major fault-bounded blocks to deform anelastically.

10 THICKNESS OF THE ELASTIC CORE

In a number of regions the observed seismicity is sufficient to constrain the depth and thickness of the apparently unbroken elastic core within the lithosphere (see Fig. 15). In this section it is assumed that the closest approach of compressional and extensional seismicity places an upper bound on the thickness of the elastic layer separating the two (where the stresses do not exceed the stress required to cause failure in earthquakes). Further, as yet unobserved, earthquakes can of course narrow this region.

The curvature of the downgoing plate as a function of distance from the trench is, in cases where the top and bottom are deforming plastically rather than elastically, directly dependent on the stress gradient within this elastic core (see Fig. 17). This gradient $(\sigma(z_1) - \sigma(z_2))/(z_1 - z_2))$ is governed by

$$\frac{\mathrm{d}^2 w}{\mathrm{d}x^2} = \frac{-(\sigma(z_1) - \sigma(z_2))(1 - \nu^2)}{E(z_1 - z_2)}, \tag{4}$$

where w is the deflection of the plate, z_1 and z_2 are the depths to the top and bottom of the elastic core, and $\sigma(z)$ is a function describing the variation in yield stress with depth (M$^{\mathrm{c}}$Adoo *et al.* 1978). $E = 8 \times 10^{10}$ Pa is the Young's modulus, and $\nu = 0.25$ the Poisson's ratio. Hence, if limits can be placed on the thickness of the core, and the curvature of the plate ($\frac{d^2w}{dx^2}$) can be estimated, it is possible to estimate the stress gradient in the elastic core. Previous studies have focused on relating the curvature at the point between the outer rise and trench where the deflection of the plate is zero, and the amplitude of the forebulge at the outer rise, to the mechanical properties and strength of the lithosphere using a set of empirically derived relations (M$^{\mathrm{c}}$Nutt & Menard 1982; M$^{\mathrm{c}}$Nutt 1984). Here, a different approach is taken, estimating the curvature of the downgoing plate using the bathymetry, low-pass filtered to remove the influence of individual faults and minor seamounts (e.g. Fig. 18a). The bathymetry is then differentiated along an azimuth perpendicular to the local trench orientation, initially to recover the gradient in the arc-wards direction (e.g. Fig. 18b), and then again to recover the curvature (e.g. Fig. 18c). Profiles perpendicular to the trench are then stacked and averaged as a function of distance from the trench (e.g. Fig. 18d). The peak mean outer-trench-slope curvature in the region seawards of the trench is then extracted. Fig. 18(e) shows the effect of applying various filters to the initial bathymetric data. For the Middle America trench (Fig. 18), when low-pass filtered at >20 km and beyond, a smooth slope in the curvature unaffected by individual faults can be seen, decreasing to zero at ∼80 km from the trench. The maximum observed curvature is taken from the calculation performed with a filter width of 20 km. This may represent a slight underestimate of the true maximum curvature, as values close to the trench are influenced by the filter width. However, it is a common result to all model rheologies previously used—elastic, elastic-plastic and viscous—that a transition from bending to unbending, and hence a decrease in the observed curvature, occurs seawards of the trench (Watts & Talwani 1974; Caldwell *et al.* 1976; Chapple & Forsyth 1979). The maximum curvature point is therefore not expected to be at the trench, where the estimates used here are affected by the filter-width used. Based on the observed shape of the curvature profiles, while the peak value maybe a slight underestimate, it is unlikely to be in error by more than a factor of ∼1.5.

The observed seismicity is sufficient to provide constraints on the thickness of the elastic core ($z_1 - z_2$ in eq. 4) in a number of regions (see Fig. 15). Central America, Chile, Honshu, the Kurils and three regions along the Tonga-Kermadec subduction zone, all have

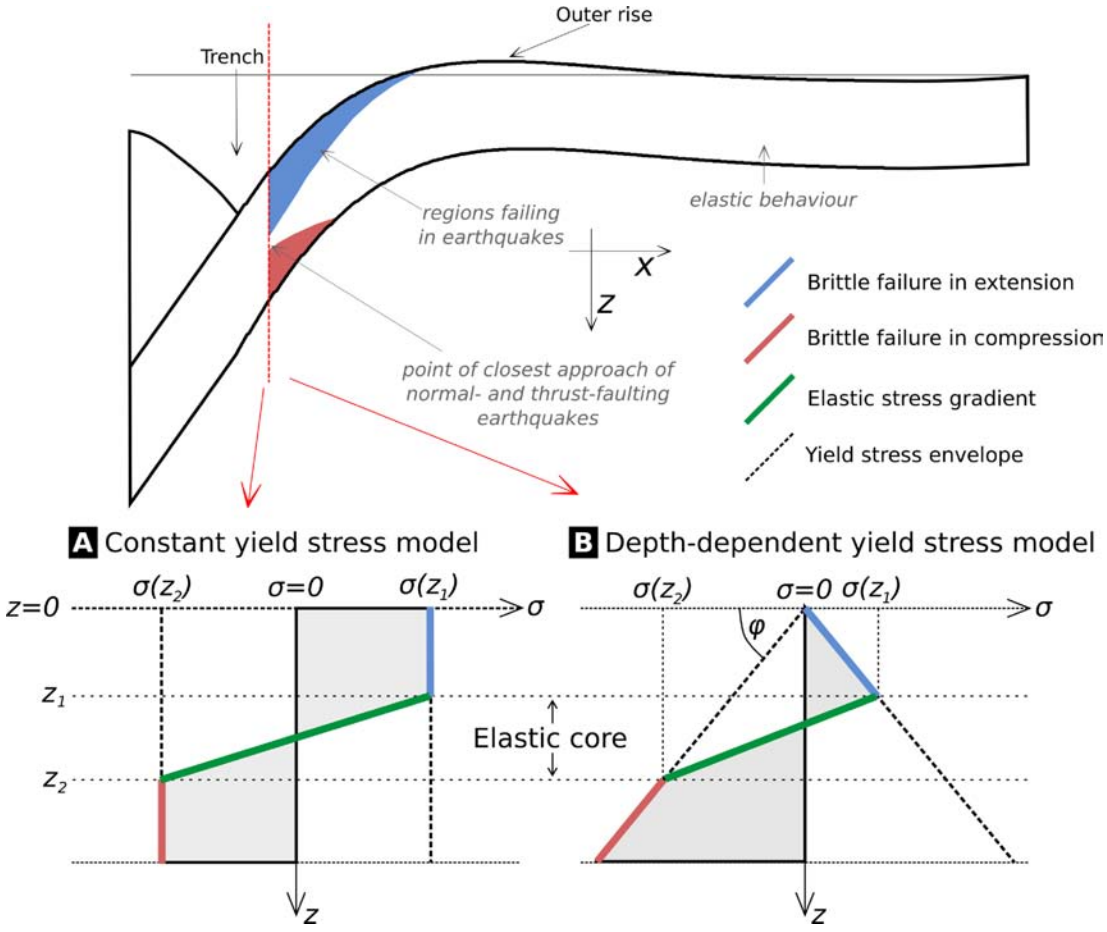

Figure 17. Sketch of the setup for the calculation of plate strength. (a) and (b) Vertical stress profiles through the point of closest approach of normal- and thrust-faulting earthquakes within the downgoing plate. (a) Constant yield stress case, and (b) the depth-dependent case governed by a uniform coefficient of friction. The plate curvature is governed by the stress gradient within the elastic core.

multiple thrust- and normal-faulting earthquakes in the same place, providing a means of estimating the elastic core width. Results from the Philippines, where the compressional region is constrained by a single earthquake only, are discarded. The Marianas arc, where the only observed compressional earthquakes strike perpendicular to the local strike of the adjacent trench, as discussed in Section 4.4, is also not included in our calculations. Together with the extreme along-strike curvature of the Marianas trench, the representation of the stress regime as two-dimensional is not appropriate in this case.

Of the seven regions with elastic core thickness estimates, curvature estimates are not possible at three of them. Estimating the curvature at the northern section of the Tonga subduction zone is complicated by subduction of local seamounts. For Chile, the trench bathymetry, gradient and curvature vary too much along strike of the trench over the region in which the earthquakes occur for a single estimate of the curvature to be valid. Additionally, any estimates of across-strike curvature are complicated by the flooding of the trench by turbidites shed from the western Andes. For the Honshu arc, curvature estimates are again complicated by structural features on the incoming plate. As expected for the region with the deepest well-constrained elastic core (Fig. 15), Honshu also has the thickest layer failing in tension by faulting, and hence can sustain the highest-offset faults. Indeed, major normal faults in the outer trench slope off Honshu often have very large offsets, up to several hundred metres, and wide fault spacings (Masson 1991; Kobayashi *et al.* 1998; Nakamura *et al.* 2013). The scale of faulting makes it very difficult to remove the effect of individual faults from estimates of the curvature, and requires filter-widths so wide that the influence of the forearc slope is smeared over significant distances seaward of the trench, resulting in large uncertainties in estimates of the maximum curvature. As a result, the Honshu arc is also excluded from quantitative analysis.

Table 1 gives the seismological constraints on the elastic core, estimated peak curvature, and the stress difference across the elastic core, from eq. (4). Results are calculated for two simple rheological models: one in which the yield stress is constant with depth, and another in which the yield stress varies linearly with depth as a function of an effective coefficient of friction. These models are detailed in Fig. 17. The calculation of stresses at the top and base of the elastic core follows directly from eq. (4). In the case of the depth-dependent model, the coefficient of friction (μ) is then calculated using

$$\Delta\sigma_{xx} = \frac{2\mu\rho g z}{\sin(2\theta) - \mu(1+\cos(2\theta))} \quad (5)$$

(Turcotte & Schubert 2002), assuming a fault dip (θ) of 45°, and a density (ρ) of 3300 kg m^{-3}.

Notably, the yield stresses estimated from both constant-yield-stress and depth-dependent models are similar—all are on the order of 100–400 MPa. For the depth-dependent model, the estimated bounds on the effective coefficients of friction vary from 0.09 (the Kurils) to 0.35 (Middle America). Given that further earthquakes

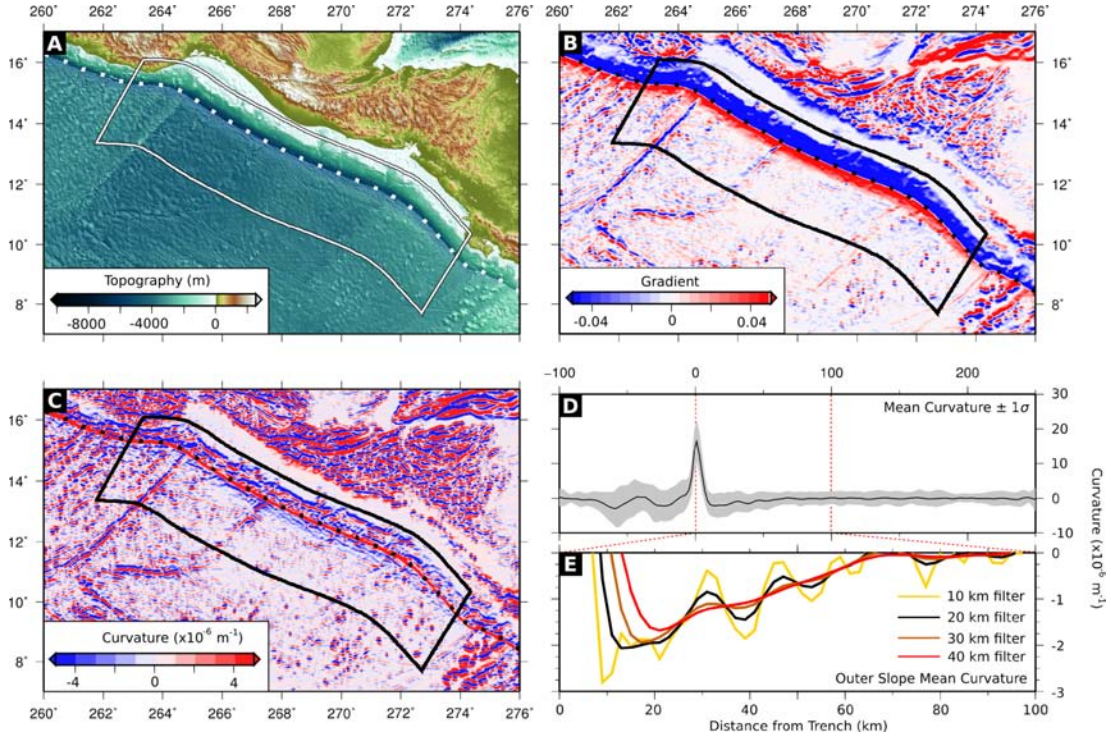

Figure 18. Estimating the curvature of the Middle America trench. (a) Unfiltered SRTM30PLUS topography and bathymetry. Swath area is outlined in white. (b) Gradient along an azimuth of 30°E of topography filtered at wavelengths of 20 km. Swath area is outlined in black. (c) Curvature along an azimuth of 30°E of topography filtered at wavelengths of 20 km. Swath area is outlined in black. (d) Mean $\pm 1\sigma$ curvature within the swath area as a function of distance from the trench for topography filtered at 20 km along a 30°E azimuth. (e) Mean outer-trench-slope curvature, evaluated using different topographic filters.

Table 1. Stress and friction results for constrained elastic cores. z_1, depth of deepest extensional earthquake; z_2, depth of shallowest compressional earthquake; $\frac{d^2w}{dx^2}$, curvature; x_{filter}, the width of filter applied to the bathymetry in estimating the curvature, tailored to remove the influence of individual faults in each case; σ_0, yield stress for a constant yield stress model; μ, the coefficient of friction estimated for a depth-dependent yield stress model; σ_{z_1}, yield stress at the top of the elastic core in the depth-dependent model; σ_{z_2}, the yield stress at the base of the elastic core in the depth-dependent yield stress model.

	Elastic core results								
Region	z_1 (km)	z_2 (km)	$z_2 - z_1$ (km)	$\frac{d^2w}{dx^2}$ (μm^{-1})	x_{filter} (km)	σ_0 (MPa)	μ	σ_{z_1} (MPa)	σ_{z_2} (MPa)
M. America	10	15	5	2.02	20	431	0.35	345	517
Chile	23	28	7	–	–	–	–	–	–
Honshu	28	30	2	–	–	–	–	–	–
Kurils	22	30	8	0.46	40	157	0.09	133	181
N. Tonga	13	20	7	–	–	–	–	–	–
C. Tonga	23	30	7	0.92	30	274	0.14	238	310
S. Tonga	26	30	4	1.11	30	189	0.09	175	202

can narrow the thickness of the elastic core, the values for the yield stress and effective coefficient of friction presented here represent upper bounds on what is possible, and are not actual estimates of the value of these parameters. Notably, even if the estimates of the curvature are out by a factor of 1.5, and the elastic core is widened by the error bounds of the earthquake depths, to provide a maximum upper limit, the coefficients of friction estimated for the Kurils, central Tonga and for southern Tonga only increase from 0.09, 0.14 and 0.09 to 0.19, 0.31 and 0.28, respectively, although the value for Middle America increases from 0.35 to 0.64. With the exception of Middle America, these values for the effective coefficient of friction, upper bounds though they are, are still significantly below the value of 0.6 typically assumed for geological materials (Byerlee 1978). They are, however, compatible with more recent estimates of the effective coefficient of friction on active faults which range from 0.04 to 0.1 (Lamb 2006; Herman *et al.* 2010; Copley *et al.* 2011). The lower bound on these estimates is effectively unconstrained, due to the potential for further earthquakes to continue to narrow the observed core. It is also important to note that the seismological results of the work, and this calculation, assume the representation of the earthquakes as a point source, rather than considering their finite extent. Consideration of the finite extent of the earthquake rupture will further narrow the elastic core, and decrease our estimates for the stresses supported by the lithosphere. For the majority of earthquakes considered, this depth extent of rupture will likely be similar to the magnitude of the depth uncertainty in the centroid,

but is difficult to calculate precisely without knowing the earthquake stress drop.

Previous studies have suggested that faulting in outer-rise settings plays a role in permitting the penetration of fluids deep into the mantle lithosphere of the subducting slab, on the assumption that the lower plane in intraslab double seismic zones downdip of the trench results from dehydration reactions (Peacock 2001), although this hypothesis is only one of a number of possible explanations for such earthquakes (e.g. Kelemen & Hirth 2007). The presence of significant fluid injection along outer-rise faults, and the formation of hydrous mineral phases, would lower the effective coefficient of friction on the faults considerably. However, the presence of an elastic core separating regions of normal faulting from deeper thrust faulting would be likely to inhibit the penetration of fluids into the deeper parts of the plate. While mineral alteration may be related to the low values for the yield stress and effective coefficient of friction found here, the correspondence of these values with those estimated from elsewhere suggests that outer rises are not significantly weaker than is typical. An alternative explanation for the low stresses we infer is that the faults are weakened by the presence of pressurized pore-fluids, lowering the limiting deviatoric stress that must be overcome for slip to occur.

11 CONCLUSIONS

The expanded database of outer-rise seismicity presented here illuminates a number of key points concerning the seismicity in the downgoing oceanic plate seawards of subduction zones.

(i) Oceanic intraplate seismicity is uniformly confined to regions expected to be colder than ∼600 °C, in agreement with the previous findings of M^{c}Kenzie *et al.* (2005). Nowhere do earthquake centroids indicate seismicity occurring at hotter temperatures within the oceanic mantle.

(ii) In all cases, a vertical separation is seen between shallow normal-faulting earthquakes, and, where present, deeper thrust-faulting earthquakes, with a narrow aseismic region separating the two.

(iii) Where only normal faulting has been observed, earthquakes appear to be restricted to shallower depths. Beneath some is a region colder than 600 °C, which is expected to be capable of brittle failure, but in which no earthquakes have been observed. This lack of seismicity may indicate that the bending stresses are supported elastically, or may simply be the result of the short duration of the observation period relative to the length of the seismic cycle.

(iv) No temporal variation is seen in the depth of the transition between shallow normal faulting and deeper thrust faulting, and no location has been observed to fail in both horizontal compression and horizontal extension across the interface seismic cycle.

(v) Relative changes in the depth of the unbroken elastic core, the aseismic region separating shallow normal faulting from deeper thrust faulting, may result from variations in slab pull, resistance to slab penetration through the 660 km discontinuity, the dip of the subducting slab, the degree of stress transfer across the interface, and in-plane forces in the incoming plate arising from ridge push, thermal contraction and dynamic topography.

(vi) Surface strain accumulated on major faults is similar to that predicted based on the depth of the elastic core, in agreement with the largest earthquakes making up the majority of the seismic moment release. However, anelastic internal deformation of the fault blocks is required to support the large-scale surface offsets observed on the largest faults, which must decrease to zero at the depth of the elastic core.

(vii) Typical elastic core thicknesses, constrained by the separation of earthquakes accommodating opposite senses of deformation, are $\leq$8 km.

(viii) Estimates of the strength of faults within the oceanic lithosphere, based on the thickness of the elastic core and estimates of the curvature suggest that the faults are typically weak, with average uniform failure stresses of $\lesssim$300 MPa, or an effective coefficient of friction of $\lesssim$0.3.

ACKNOWLEDGEMENTS

Seismogram data were retrieved from the IRIS Data Management Centre. A number of figures were made using GMT (Wessel & Smith 1998). TJC was funded by a Girdler scholarship from the University of Cambridge and a NERC studentship. AC and JJ acknowledge support through the NERC- and ESRC-funded ‘Earthquakes without Frontiers’ project. We thank Thorne Lay and two anonymous reviewers, along with the editor, Ingo Grevemeyer, for their comments, which helped improve the manuscript.

REFERENCES

Abe, K., 1972. Lithospheric normal faulting beneath the Aleutian Trench, *Phys. Earth planet Inter.*, **5,** 190–198.

Abercrombie, R.E. & Ekstrom, G., 2001. Earthquake slip on oceanic transform faults, *Nature*, **410,** 74–77.

Ammon, C.J., Kanamori, H. & Lay, T., 2008. A great earthquake doublet and seismic stress transfer cycle in the central Kuril islands, *Nature*, **451,** 561–567.

Bai, L., Bergman, E.A., Engdahl, E.R. & Kawasaki, I., 2007. The 2004 earthquakes offshore of the Kii peninsula, Japan: hypocentral relocation, source process and tectonic implications, *Phys. Earth planet. Inter.*, **165,** 47–55.

Boettcher, M.S., Hirth, G. & Evans, B., 2007. Olivine friction at the base of oceanic seismogenic zones, *J. geophys. Res.*, **112,** doi:10.1029/2006JB004301.

Byerlee, J., 1978. Friction of rocks, *Pure appl. Geophys.*, **116,** 615–626.

Caldwell, J.G., Haxby, W.F., Karig, D.E. & Turcotte, D.L., 1976. On the applicability of a universal elastic trench profile, *Earth planet. Sci. Lett.*, **31,** 239–246.

Chamot-Rooke, N. & Le Pichon, X., 1989. Zenisu Ridge: mechanical model of formation, *Tectonophysics*, **160,** 175–193.

Chapman, C., Yen-Li, C. & Lyness, D., 1988. The WKBJ seismogram algorithm, in *Seismological Algorithms: computational Methods and Computer Programs*, pp. 47–74, ed. Doornbos, D., Academic Press Limited.

Chapple, W.M. & Forsyth, D.W., 1979. Earthquakes and bending of plates and trenches, *J. geophys. Res.*, **84,** 6729–6749.

Chen, T. & Forsyth, D.W., 1979. A detailed study of two earthquakes seaward of the Tonga Trench: implications for mechanical behaviour of the oceanic lithosphere, *J. geophys. Res.*, **83,** 4995–5003.

Chinn, D.S. & Isacks, B.L., 1983. Accurate source depths and focal mechanisms of shallow earthquakes in western South America and in the New Hebrides Island Arc, *J. geophys. Res.*, **2,** 529–563.

Christensen, D.H. & Ruff, L.J., 1983. Outer-rise earthquakes and seismic coupling, *Geophys. Res. Lett.*, **10,** 697–700.

Christensen, D.H. & Ruff, L.J., 1988. Seismic coupling and outer rise earthquakes, *J. geophys. Res.*, **93,** 13 421–13 444.

Copley, A., Avouac, J.-P., Hollingsworth, J. & Leprince, S., 2011. The 2001 M_w 7.6 Bhuj earthquake, low fault friction, and the crustal support of plate driving forces in India, *J. geophys. Res.*, **116,** doi:10.1029/2010JB008137.

Crosby, A.G., M^{c}Kenzie, D. & Sclater, J.G., 2006. The relationship between depth, age and gravity in the oceans, *Geophys. J. Int.*, **166,** 553–573.

DeMets, C., Gordon, R.G. & Angus, D.F., 2010. Geologically current plate motions, *Geophys. J. Int.*, **181,** 1–80.

Denlinger, R.P., 1992. A revised estimate for the temperature structure of the oceanic lithosphere, *J. geophys. Res.*, **97,** 7219–7222.

Dewey, J.W., Choy, G., Presgrave, B., Sipkin, S., Tarr, A.C., Benz, H., Earle, P. & Wald, D., 2007. Seismicity associated with the Sumatra-Andaman Islands earthquake of 26 December 2004, *Bull. seism. Soc. Am.*, **97,** S25–S42.

Eissler, H. & Kanamori, H., 1982. A large normal-fault earthquake at the junction of the Tonga trench and the Louisville ridge, *Phys. Earth planet. Inter.*, **29,** 161–172.

Engdahl, E.R., van der Hilst, R.D. & Buland, R.P., 1998. Global teleseismic earthquake relocation with improved travel times and prceedures for depth determination, *Bull, seism. Soc. Am.*, **88,** 722–743.

Fitch, T.J., North, R.G. & Shields, M.W., 1981. Focal depths and moment tensor representations of shallow earthquakes associated with the great Sumba earthquake, *J. geophys. Res.*, **86,** 9357–9374.

Forsyth, D.W., 1980. Comparison of mechanical models of the oceanic lithosphere, *J. geophys. Res.*, **85,** 6364–6368.

Forsyth, D.W., 1982. Determinations of focal depths of earthquakes associated with the bending of oceanic plates at trenches, *Phys. Earth planet. Inter.*, **28,** 141–160.

Forsyth, D. & Uyeda, S., 1975. On the relative importance of the driving forces of plate motion, *Geophys. J. R. astr. Soc.*, **43,** 163–200.

Gamage, S.S.N., Umino, N., Hasegawa, A. & Kirby, S.H., 2009. Offshore double-planed shallow seismic zone in the NE Japan forearc region revealed by sP depth phases recorded by regional networks, *Geophys. J. Int.*, **178,** 195–214.

Harada, T., Murotani, S. & Satake, K., 2013. A deep outer-rise reverse-fault earthquake immediately triggered a shallow normal-fault earthquake: the 7 December 2012 off-Sanriku earthquake (M_W 7.3), *Geophys. Res. Lett.*, **40,** 4214–4219.

Hayes, G.P., Wald, D.J. & Johnson, R.L., 2012. Slab1.0: a three-dimensional model of global subduction zone geometries, *J. geophys. Res.*, **117,** doi:10.1029/2011JB008524.

Herman, F. *et al.*, 2010. Exhumation, crustal deformation, and thermal structure of the Nepal Himalaya derived from the inversion of thermochronological and thermobarometric data and modeling of the topography, *J. geophys. Res.*, **115,** doi:10.1029/2008JB006126.

Herrmann, R.B., 1976. Focal depth determination from the signl character of long-period *P* waves, *Bull. seism. Soc. Am.*, **66,** 1221–1232.

Hino, R. *et al.*, 2009. Insight into complex rupturing of the immature bending normal fault in the outer slope of the Japan Trench from aftershocks of the 2005 Sanriku earthquake ($M_W = 7.0$) located by ocean bottom seismometry, *Geochem., Geophys., Geosyst.*, **10,** doi:10.1029/2009GC002415.

Honda, S. & Kawakatsu, H., 1990. The depth of the October 1981 off Chile outer-rise earthquake ($M_S = 7.2$) estimated by a comparison of several waveform inversion methods, *Bull. seism. Soc. Am.*, **80,** 69–87.

Isacks, B. & Molnar, P., 1971. Distribution of stresses in the descending lithosphere from a global survey of focal-mechanism solutions of mantle earthquakes, *Rev. Geophys. Space Phys.*, **9,** 103–175.

Jackson, J., M^{c}Kenzie, D., Priestley, K. & Emmerson, B., 2008. New views on the structure and rheology of the lithosphere, *J. geol. Soc. Lond.*, **165,** 453–465.

Jarrard, R., 1986. Relations among subduction parameters, *Rev. Geophys.*, **24,** 771–778.

Jaumé, S.C. & Estabrook, C.H., 1992. Accelerating seismic moment release and outer-rise compression: possible precursors to the next great earthquake in the Alaska Peninsula region, *Geophys. Res. Lett.*, **19,** 345–348.

Kanamori, H., 1971. Seismological evidence for a lithospheric normal faulting – the Sanriku earthquake of 1933, *Phys. Earth planet. Inter.*, **4,** 289–300.

Kanamori, H., 1972. Mechanism of tsunami earthquakes, *Phys. Earth planet. Inter.*, **6,** 346–359.

Kao, H. & Chen, W.-P., 1991. Earthquakes along the Ryukyu-Kyushu Arc: strain segmentation, lateral compression and the thermomechanical state of the plate interface, *J. geophys. Res.*, **96,** 21 443–21 485.

Kelemen, P. & Hirth, G., 2007. A periodic shear-heating mechanism for intermediate-depth earthquakes in the mantle, *Nature*, **446,** doi:10.1038/nature05717.

Kobayashi, K., Nakanishi, M., Tamaki, K. & Ogawa, Y., 1998. Outer slope faulting associated with the western Kurils and Japan trenches, *Geophys. J. Int.*, **134,** 356–372.

Korrat, I. & Madariaga, R., 1986. Rupture of the Valpariso (Chile) gap from 1971 to 1986, in *Earthquake Source Mechanics, Geophysical Monograph*, Vol. **6,** pp. 247–258, eds Das, S., Boatwright, J. & Scholz, C.H., American Geophysical Union.

Lallemant, S., Chamot-Rooke, N., Le Pichon, X. & Rangin, C., 1989. Zenisu Ridge: a deep intraoceanic thrust related to subduction, off southwest Japan, *Tectonophysics*, **160,** 151–174.

Lamb, S., 2006. Shear stresses on megathrusts: implications for mountain building behind subduction zones, *J. geophys. Res.*, **111,** doi:10.1029/2005JB003916.

Lay, T., Astiz, L., Kanamori, H. & Christensen, D.H., 1989. Temporal variation of large intraplate earthquakes in coupled subduction zones, *Phys. Earth planet. Inter.*, **54,** 258–312.

Lay, T., Kanamori, H., Ammon, C.J., Hutko, A.R., Furlong, K. & Rivera, L., 2009. The 2006-2007 Kuril Islands great earthquake sequence, *J. geophys. Res.*, **114,** doi:10.1029/2008JB006280.

Lay, T., Ammon, C.J., Kanamori, H., Rivera, L., Koper, K.D. & Hutko, A.R., 2010. The 2009 Samoa-Tonga great earthquake triggered doublet, *Nature*, **466,** doi:10.1038/nature09214.

Lay, T., Ammon, C.J., Kanamori, H., Kim, M.J. & Xue, L., 2011. Outer trench-slope faulting and the 2011 M_W 9.0 off the Pacific coast of Tohoku Earthquake, *Earth Planets Space*, **63,** 713–718.

Lay, T., Duputel, Z., Ye, L. & Kanamori, H., 2013. The December 7, 2012 Japan Trench intraplate doublet (M_W 7.2, 7.1) and interactions between near-trench intraplate thrust and normal faulting, *Phys. Earth planet. Inter.*, **220,** 73–78.

Lefeldt, M., Grevemeyer, I.J. & Goßler Bialas, J., 2009. Intraplate seismcity and related mantle hydration at the Nicaraguan trench outer rise, *Geophys. J. Int.*, **178,** 742–752.

Liu, X. & M^{c}Nally, K.C., 1993. Quantitative estimates of interplate coupling inferred from outer rise earthquakes, *Pure appl. Geophys.*, **140,** 211–255.

Lynnes, C.S. & Lay, T., 1988. Source process of the great 1977 Sumba earthquake, *J. geophys. Res.*, **93,** 13 407–13 420.

Mahadevan, L., Bendick, R. & Liang, H., 2010. Why subduction zones are curved, *Tectonics*, **29,** doi:10.1020/2010TC002720.

Masson, D.G., 1991. Fault patterns at outer trench walls, *Marine Geophys. Res.*, **13,** 209–225.

M^{c}Adoo, D.C., Caldwell, J.G. & Turcotte, D.L., 1978. On the elastic-perfectly plastic bending of the lithosphere under generalised loading with application to the Kuril Trench, *Geophys. J. R. astr. Soc.*, **54,** 11–26.

M^{c}Kenzie, D., 1969. Speculations on the consequences and causes of plate motions, *Geophys. J. R. astr. Soc.*, **18,** 1–32.

M^{c}Kenzie, D., Jackson, J. & Priestley, K., 2005. Thermal structure of oceanic and continental lithosphere, *Earth planet. Sci. Lett.*, **233,** 337–349.

M^{c}Nutt, M.K., 1984. Lithospheric flexure and thermal anomalies, *J. geophys. Res.*, **89,** 11 180–11 194.

M^{c}Nutt, M.K. & Menard, H.W., 1982. Constraints on yield strength in the oceanic lithosphere derived from observations of flexure, *Geophys. J. R. astr. Soc.*, **71,** 363–394.

Muller, R.D., Sdrolias, M., Gaina, C. & Roest, W.R., 2008. Age, spreading rates, and spreading asymmetry of the world's ocean crust, *Geochem., Geophys., Geosyst.*, **9,** doi:10.1029/2007GC001743.

Nakamura, Y., Kodaira, S., Miura, S., Regalla, C. & Takahashi, N., 2013. High-resolution seismic imaging in the Japan Trench axis area off Miyagi, northeastern Japan, *Geophys. Res. Lett.*, **40,** doi:10.1002/grl.50364.

Obana, K.M. *et al.*, 2012. Normal-faulting earthquakes beneath the outer slope of the Japan Trench after the 2011 Tohoku earthquake: implications for the stress regime in the incoming Pacific plate, *Geophys. Res. Lett.*, **39,** doi:10.1029/2011GL050399.

Parsons, B. & Richter, F.M., 1980. A relation between the driving force and geoid anomaly associated with mid-ocean ridges, *Earth planet. Sci. Lett.*, **51,** 445–450.

Parsons, B. & Sclater, J.G., 1977. An analysis of the variation of ocean floor bathymetry and heat flow with age, *J. geophys. Res.*, **82,** 803–827.

Peacock, S.M., 2001. Are the lower planes of double seismic zones caused by serpentine dehydration in subducting oceanic mantle? *Geology,* **29,** 299–302.

Pesicek, J.D., Thurber, C H., Zhang, H., DeShon, H. R., Engdahl, E.R. & Widiyantoro, S., 2010. Teleseismic double-difference relocation of earthquakes along the Sumatra-Andaman subduction zone using a 3-D model, *J. geophys. Res.*, **115,** doi:10.1029/2010JB007443.

Raeesi, M. & Atakan, K., 2009. On the deformation cycle of a strongly coupled plate interface: the triple earthquakes of 16 March 1963, 15 November 2006 and 13 January 2007 along the Kurile subduction zone, *J. geophys. Res.*, **114,** doi:10.1029/2008JB006184.

Ranero, C.R., Phipps Morgan, J., M^{c}Intosh, K. & Reichert, C., 2003. Bending-related faulting and mantle serpentinization at the Middle America trench, *Nature,* **425,** 367–374.

Rhea, S., Hayes, G., Villaseñor, A., Furlong, K.P., Tarr, A.C. & Benz, H.M., 2010. Seismicity of the Earth, 1900-2007, Open-File Report 2010-1083, United States Geological Survey.

Ruff, L. & Kanamori, H., 1980. Seismicity and the subduction process, *Phys. Earth planet. Inter.*, **23,** 240–252.

Sakai, S., Yamada, T., Shinohara, M., Hagiwara, H., Kanazawa, T., Obana, K., Kodaira, S. & Kaneda, Y., 2005. Urgent aftershock observation of the 2004 off the Kii Peninsula earthquake using ocean bottom seismometers, *Earth Planets Space,* **57,** 363–368.

Seno, T. & Gonzalez, D.G., 1987. Faulting caused by earthquakes beneath the outer slope of the Japan Trench, *J. Phys. Earth,* **35,** 381–407.

Seno, T. & Yamanaka, Y., 1996. Double seismic zones, compressional deep trench-outer rise events, and superplumes, in *Subduction: top to Bottom, Geophysical Monograph,* Vol. **96,** pp. 347–355. American Geophysical Union.

Shaw, B. & Jackson, J., 2010. Earthquake mechanisms and active tectonics of the Hellenic subduction zone, *Geophys. J. Int.*, **181,** 966–984.

Spence, W., 1986. The 1977 Sumba earthquake series: evidence for slab pull force acting at a subduction zone, *J. geophys. Res.*, **91,** 7225–7239.

Stauder, W., 1968a. Mechanism of the Rat Island earthquake sequence of February 1965, with relation to island arcs and sea-floor spreading, *J. geophys. Res.*, **73,** 3847–3858.

Stauder, W., 1968b. Tensional character of earthquake foci beneath the Aleutian Trench with relation to sea-floor spreading, *J. geophys. Res.*, **73,** 7693–7701.

Taymaz, T., Jackson, J. & M^{c}Kenzie, D., 1991. Active tectonics of the north and central Aegean Sea, *Geophys. J. Int.*, **106,** 433–490.

Tichelaar, B.W., Christensen, D.H. & Ruff, L.J., 1992. Depth extent of rupture of the 1981 Chilean outer-rise earthquake as inferred from long-period body waves, *Bull. seism. Soc. Am.*, **82,** 1236–1252.

Tilmann, F.J., Grevemeyer, I., Flueh, E.R., Dahm, T. & Goßler, J., 2008. Seismicity in the outer rise offshore southern Chile: indication of fluid effects in crust and mantle, *Earth planet. Sci. Lett.*, **269,** 41–55.

Tilmann, F.J., Craig, T.J., Grevemeyer, I., Suwargadi, B., Kopp, H. & Flueh, E., 2010. The updip seismic/aseismic transition of the Sumatra megathrust illuminated by aftershocks of the 2004 Aceh-Andaman and 2005 Nias events, *Geophys. J. Int.*, **181,** 1261–1274.

Todd, E.K. & Lay, T., 2013. The 2011 Northern Kermadec earthquake doublet and subduction zone faulting interactions, *J. geophys. Res.*, **118,** 1–13.

Turcotte, D. & Schubert, G., 2002. *Geodynamics*, Cambridge University Press.

Vallée, M., Bouchon, M. & Schwartz, S.Y., 2003. The 13 January 2001 El Salvador earthquake: a multidata analysis, *J. geophys. Res.*, **108,** doi:10.1029/2002JB001922.

Wang, K., Mulder, T., Rogers, G.C. & Hyndman, R.D., 1995. Case for very low coupling stress on the Cascadia subduction fault, *J. geophys. Res.*, **100,** 12 907–12 918.

Watts, A.B. & Talwani, M., 1974. Gravity anomalies seaward of deep-sea trenches and their tectonic implications, *Geophys. J. R. astr. Soc.*, **36,** 57–90.

Webb, T.H. & Anderson, H., 1998. Focal mechanisms of large earthquakes in the North Island of New Zealand: slip partitioning at an oblique active margin, *Geophys. J. Int.*, **134,** 40–86.

Wessel, P. & Smith, W.H.F., 1998. New, improved version of Generic Mapping Tools released, *EOS, Trans. Am. geophys. Un.*, **79,** 579.

Wiens, D.A. & Stein, S., 1983. Age dependence of oceanic intraplate seismicity and implications for lithospheric evolution, *J. geophys. Res.*, **88,** 6455–6468.

Winterbourne, J., Crosby, A. & White, N., 2009. Depth, age and dyamic topography of oceanic lithosphere beneath heavily sedimented Atlantic margins, *Earth planet. Sci. Lett.*, **287,** 137–151.

Ye, L., Lay, T. & Kanamori, H., 2012. Intraplate and interplate faulting interactions during the August 31, 2012, Philippine Trench earthquake (M_W 7.6) sequence, *Geophys. Res. Lett.*, **39,** doi:10.1029/2012GL054164.

Yue, H. & Lay, T., 2011. Inversion of high-rate (1 sps) GPS data for rupture process of the 11 March 2011 Tohoku earthquake (M_W 9.1), *Geophys. Res. Lett.*, **38,** doi:10.1029/2011GL048700.

Zhang, J. & Lay, T., 1992. The April 5, 1990 Mariana Islands earthquake and subduction zone stresses, *Phys. Earth planet. Inter.*, **72,** 99–121.

Zwick, P., M^{c}Caffrey, R. & Abers, G., 1994. MT5 program, *IASPEI Software Library,* **4**.

SUPPORTING INFORMATION

Additional Supporting Information may be found in the online version of this article:

Figure S1: Profiles of outer-rise seismicity and morphology.
Figure S2: New waveform modelling solution for the 1964 August 18 Chilean earthquake.
Table S1: Waveform modelling results for outer-rise earthquakes from this study.
(http://mnras.oxfordjournals.org/lookup/suppl/doi:10.1093/gjiras/ggu013/-/DC1).

Please note: Oxford University Press is not responsible for the content or functionality of any supporting materials supplied by the authors. Any queries (other than missing material) should be directed to the corresponding author for the article.